RESEARCH ARTICLE SUMMARY

BRAIN EVOLUTION

Evolutionary convergence of sensory circuits in the pallium of amniotes

Eneritz Rueda-Alaña, Rodrigo Senovilla-Ganzo, Marco Grillo, Enrique Vázquez, Sergio Marco-Salas, Tatiana Gallego-Flores, Aitor Ordeñana-Manso, Artemis Ftara, Laura Escobar, Alberto Benguría, Ana Quintas, Ana Dopazo, Miriam Rábano, María dM Vivanco, Ana María Aransay, Daniel Garrigos, Ángel Toval, José Luis Ferrán, Mats Nilsson, Juan Manuel Encinas-Pérez, Maurizio De Pittà, Fernando García-Moreno*

INTRODUCTION: For decades, scientists have debated the homologies between the mammalian neocortex and the pallium of other vertebrates. Claims of homology are often based on gene expression patterns in embryonic brains or neuronal connectivity patterns in adult brains. We sought to understand pallial evolution because its homologies provide insights into the evolutionary and developmental pathways of brain structures across species.

RATIONALE: We tackled this debate from alternative perspectives by investigating the developmental formation of pallial circuitry through neurogenic, transcriptional, and mathematical analyses in three selected species: chick, mouse, and gecko. By examining the development of their pallial circuits, we aimed to determine whether similarities in sensory processing circuits are due to conserved homology or convergent evolution.

RESULTS: Our study revealed that neurons that form the three stations of the pallial circuit are generated at different times and in distinct brain regions across species. The avian dorsal ventricular ridge (DVR) circuit develops in a different order than the neocortical circuit, whereas the avian hyperpallial circuit follows previously unknown neurogenic rules that are not seen in either the avian DVR or the mouse neocortex. Geckos exhibit a dual sequence: Their dorsal circuit forms like the mammalian neocortex, whereas their ventral circuit develops like the avian DVR. These findings indicate unexpected diversification in amniote pallial sensory circuit developmental programs.

On the molecular level, single-cell RNA sequencing depicted different evolutionary trends for equivalent cell types, produced in homologous pallial regions and at equivalent neurogenic times. Glutamatergic pallial neurons mature into divergent neuronal types in chick and mouse, whereas γ-aminobutyric acid–releasing (GABAergic) pallial neurons showed strong conservation, underscoring their fundamental role in pallial sensory circuits.

By means of spatially resolved transcriptomic analysis, we inferred the pallial location and transcriptional type of early neurons generated in the pallium of both chick and mouse. This analysis showed greater conservation of GABAergic cells and indicated that the only similarity in the glutamatergic class was mesopallial neurons of the chick brain and deep, lateral mammalian cortical neurons.

The developmental differences were also notable in progenitors and other cells. Whereas pallial radial glial cells displayed similarities between species, their neurogenic behaviors differed markedly. Additionally, the population of intermediate progenitor cells that expanded neuronal numbers in the mammalian neocortex had no clear homolog in the avian developing pallium. Cajal-Retzius cells were not found in the chick pallium. Furthermore, mathematical modeling suggests that components of sensory circuits in birds and mammals were shaped by similar functional constraints.

CONCLUSION: Our study demonstrates that high-order sensory processing circuits have evolved separately in different vertebrate taxa, converging into a functionally similar circuit. The differences in the developmental rules, progenitor cells, and transcriptomic profiles support a nonhomologous character of the amniote pallial circuits. The strong conservation of GABAergic neurons indicates their crucial role in pallial sensory circuits, whereas the divergent development of glutamatergic neurons suggests a flexible evolution of this neuronal class. Evolution tinkered with pallial circuit development, structure, and function. And likely, convergent evolution sculpted the formation of the components of the sensory circuits in amniote species. ■

The list of author affiliations is available in the full article online.
***Corresponding author. Email: fernando.garcia-moreno@achucarro.org**
Cite this article as E. Rueda-Alaña *et al.*, *Science* 387, eadp3411 (2025). DOI: 10.1126/science.adp3411

READ THE FULL ARTICLE AT
https://doi.org/10.1126/science.adp3411

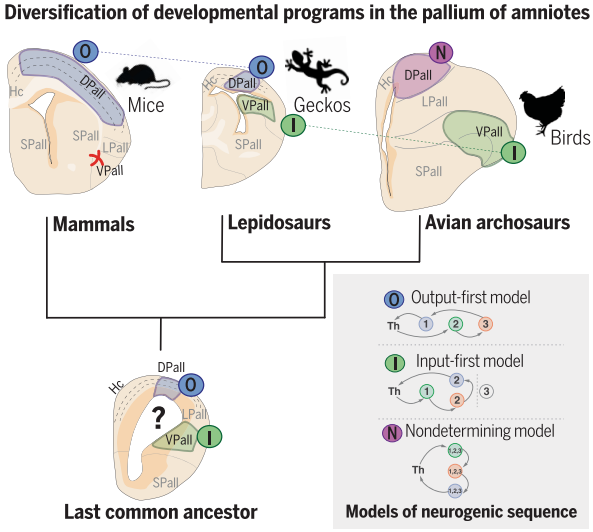

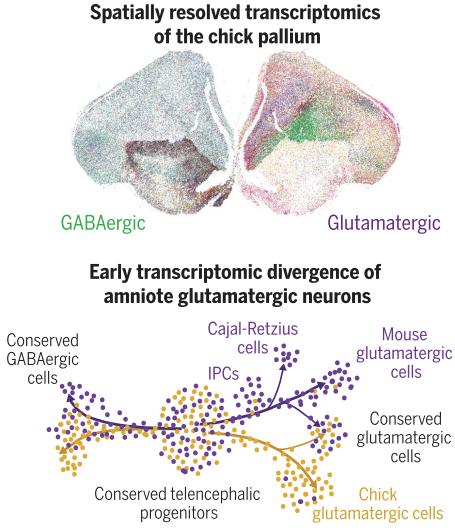

Evolutionary history of pallial development in amniotes. (Left) Illustrations depicting the varied sequences of neurogenesis found in the pallial circuits of amniotes. (Top right) Spatially resolved transcriptomics allowed us to identify a wide neuronal diversification in the chick pallium. (Bottom right) Single-cell RNA sequencing of early born neurons revealed conservation in the differentiation of GABAergic neurons in amniotes, which contrasted with the diversification of most glutamatergic neurons. DPall, dorsal pallium; Hc, hippocampus; IPCs, intermediate precursor cells; LPall, lateral pallium; SPall, subpallium; Th, thalamus; VPall, ventral pallium.

RESEARCH ARTICLE

BRAIN EVOLUTION

Evolutionary convergence of sensory circuits in the pallium of amniotes

Eneritz Rueda-Alaña[1,2], Rodrigo Senovilla-Ganzo[1,2], Marco Grillo[3], Enrique Vázquez[4], Sergio Marco-Salas[3], Tatiana Gallego-Flores[1], Aitor Ordeñana-Manso[1], Artemis Ftara[1], Laura Escobar[1], Alberto Benguría[4], Ana Quintas[4], Ana Dopazo[4,5], Miriam Rábano[6], María dM Vivanco[6], Ana María Aransay[6,7], Daniel Garrigos[8], Ángel Toval[8]†, José Luis Ferrán[8], Mats Nilsson[3], Juan Manuel Encinas-Pérez[1,2,9], Maurizio De Pittà[2,10,11,12], Fernando García-Moreno[1,2,9]*

The amniote pallium contains sensory circuits that are structurally and functionally equivalent, yet their evolutionary relationship remains unresolved. We used birthdating analysis, single-cell RNA and spatial transcriptomics, and mathematical modeling to compare the development and evolution of known pallial circuits across birds (chick), lizards (gecko), and mammals (mouse). We reveal that neurons within these circuits' stations are generated at varying developmental times and brain regions across species and found an early developmental divergence in the transcriptomic progression of glutamatergic neurons. Our research highlights developmental distinctions and functional similarities in the sensory circuit between birds and mammals, suggesting the convergence of high-order sensory processing across amniote lineages.

The neocortex is the biological substrate that underlies the sophisticated and complex functions performed by mammalian species, including humans. Neocortical neurons connect to each other following a stereotyped pattern (*1*, *2*). This canonical circuit is composed of three types of pallial glutamatergic neurons, each fulfilling a specific role in the circuitry (Fig. 1A). Electrophysiological evidence supports that these circuits account for major neocortical functions (*3*). However, vertebrate species that do not display a neocortex have similar circuitry; in both birds and reptiles, sensory information is also processed by circuits composed of three glutamatergic neurons that are contained within the pallium. The evolutionary origin of these amniote circuits is a matter of intense debate. They could be conserved homologs to neocortical circuits—and so derived from the same ancestral circuit—or analogs that have convergently evolved independently (*4*–*6*).

The three vertebrate groups—mammals (*1*), birds (*7*, *8*), and nonavian reptiles (*9*)—share equivalent circuits with potentially similar functions. Briefly, in all three groups there is a specific neuronal population that receives thalamic inputs. These neurons connect to an integrator neuron, which in turn sends its input to a third pallial neuron. This last neuron of the circuit projects the information out of the cortex, to either the thalamus, the brainstem, or other subcortical structures. Beyond similarities in their location, type of information processed, and neurotransmitters, the neuronal populations that participate in this circuitry share the expression of a handful of transcription factors (TFs), such as Tbr1, RorB, Satb2, or Ctip2 (*9*–*12*), and electrophysiological properties (*13*). Because of these functional and structural similarities (*14*), it has been suggested that all these amniote circuits are homologous (*15*), implying that an equivalent ancestral circuit was already present in the brain of the last common ancestor of amniotes around 320 million years ago. This view contrasts with evidence from developmental biology that proposes a divergent scenario for the evolution of the pallium (*16*, *17*) because these circuits appear in developmentally noncomparable brain regions.

Development and evolution are tightly linked: Variations in one dictate trends in the other (*18*, *19*). Because evolutionary homology implies inheritance from a common ancestor, the developmental trajectory must be conserved in order to argue the conservation of homologous neurons and circuits. In this work, we argue that understanding the topological developmental trajectory of a neuron or a circuit may unravel its evolutionary history (*20*, *21*). Our assumption is supported by the intimate link between neurogenesis and connectivity, as shown by the increased connectivity between sibling neurons in the cortex of mammals (*22*–*24*). Conserved homologous cell populations or circuits originate from the same neural tube region among different vertebrates that share an equivalent developmental program, as previously identified in the amniotes' cerebellar cortex (*25*). Therefore, we believe that the long-standing debate over the conservation of the sensory circuit might only be resolved by comparing the developmental trajectories of neurons according to their topological location in these amniote circuits. How did radial glial cells (RGCs) in corresponding pallial regions lead to differing neuronal structures? To investigate this evolutionary relationship and potential homology, we compared the developmental and transcriptional trajectories over the course of the early construction of pallial sensory circuits in three amniote species.

Results

Developmental neurogenesis of avian high-order sensory circuits

Conserved homologous cells share their developmental history. To test whether mammalian cortical circuits have homologous circuits in other amniote species, we determined the developmental trajectory of the pallial neurons in the sensory circuits in sauropsids. The temporal neurogenic construction of the mammalian cortical circuit is well known. By means of 5-ethynyl-2′-deoxyuridine (EdU) injections at three different time points during the neurogenic period of the chick pallium [embryonic days 4 to 9 (E4 to E9)], we revealed the temporal construction of the avian sensory circuits (Figs. 1 and 2 and figs. S1 to S11). We studied the two pallial structures that have been proposed as neocortical homologs, the dorsal ventricular ridge (DVR; Fig. 1 and figs. S1 to S6) and the hyperpallium (HPall; Fig. 2 and figs. S7 to S11). We found that none of these structures develops in an equivalent temporal sequence as that known for the mammalian cortical circuit (fig. S12).

First, we focused on the avian DVR, which was primarily considered the homolog of the neocortex according to its internal circuitry. Similarly to mammalian corticogenesis, the avian glutamatergic and γ-aminobutyric acid–releasing (GABAergic) neurons of each circuit relay were generated at the same neurogenic time (synchronously), although on different telencephalic sectors (figs. S2 to S4). Previous tracing studies revealed that most neurons of the different

[1]Achucarro Basque Center for Neuroscience, Scientific Park of the University of the Basque Country (UPV/EHU), Leioa, Spain. [2]Department of Neuroscience, Faculty of Medicine and Odontology, UPV/EHU, Barrio Sarriena s/n, Leioa, Bizkaia, Spain. [3]Science for Life Laboratory, Department of Biophysics and Biochemistry, Stockholm University, Solna, Sweden. [4]Genomics Unit, Centro Nacional de Investigaciones Cardiovasculares (CNIC), Madrid, Spain. [5]Centro de Investigación Biomédica en Red de Enfermedades Cardiovasculares (CIBERCV), Madrid, Spain. [6]Center for Cooperative Research in Biosciences (CIC bioGUNE), Basque Research and Technology Alliance (BRTA), Bizkaia Technology Park, Derio, Spain. [7]Centro de Investigación Biomédica en Red de Enfermedades Hepáticas y Digestivas (CIBERehd), Madrid, Spain. [8]Department of Human Anatomy, Medical School, University of Murcia and Murcia Arrixaca Institute for Biomedical Research, Murcia, Spain. [9]IKERBASQUE Foundation, Bilbao, Spain. [10]Basque Center for Applied Mathematics, Bilbao, Spain. [11]Computational Neuroscience Hub, Krembil Research Institute, University Health Network, Toronto, ON, Canada. [12]Department of Physiology, Temerty Faculty of Medicine, University of Toronto, Toronto, ON, Canada.
***Corresponding author. Email: fernando.garcia-moreno@achucarro.org**
†Present address: Department of Physical Education and Sports, Faculty of Sport Sciences, University of Granada, Granada, Spain.

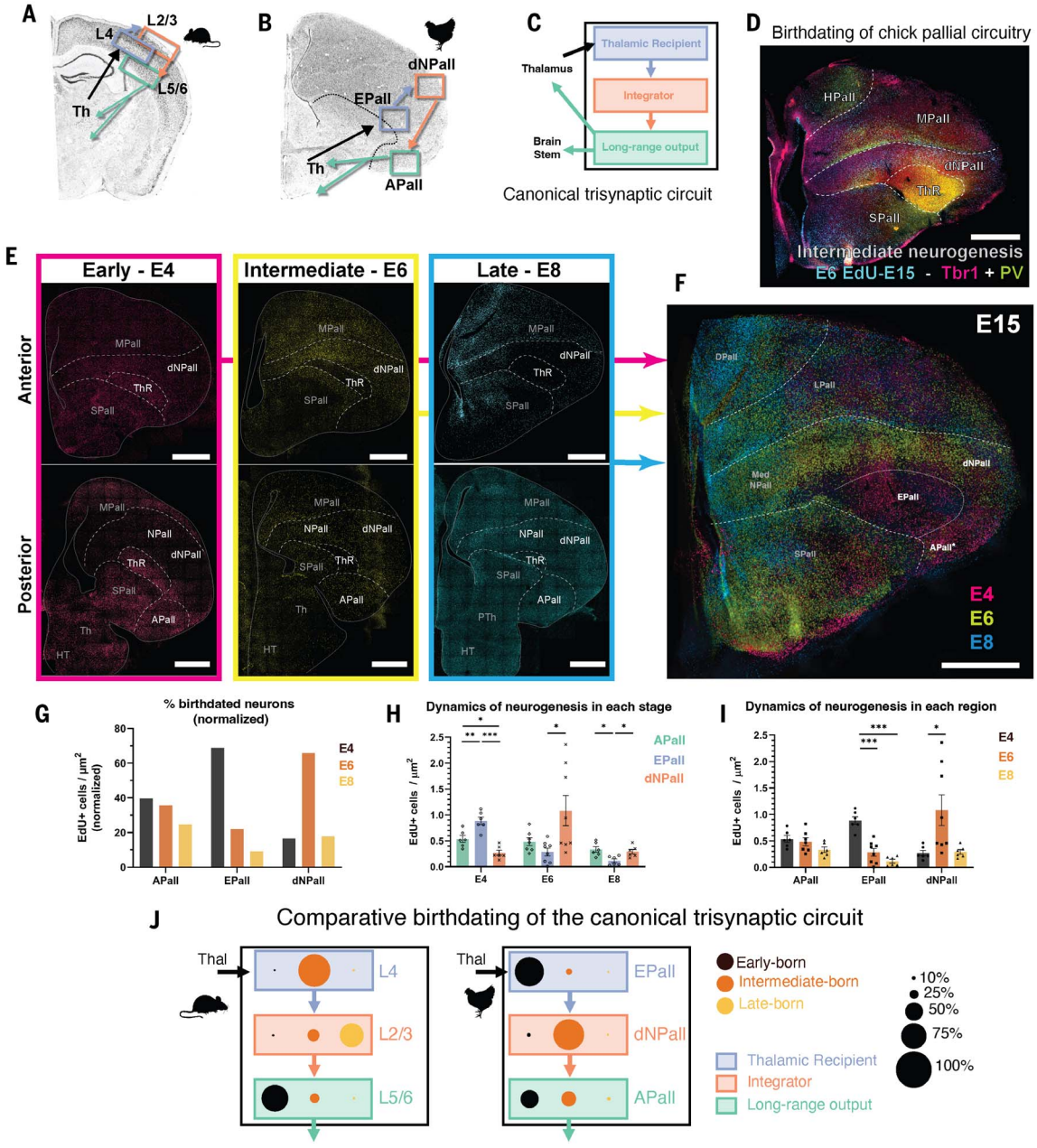

Fig. 1. Neuronal birthdating of the components of the chick DVR sensory circuit. (**A**) Schematic highlighting the connections of the mammalian cortical canonical circuit. Th, thalamus. (**B**) Equivalent schematic depicting the connections of the chick DVR canonical circuit. (**C**) Scheme of the basic cell type organization in the trisynaptic circuit of amniotes. (**D**) Example of coronal section of the chick telencephalon in a typical experiment, where EdU is labeled (cyan) along with two markers by immunohistochemistry, PV (green) and Tbr1 (magenta). ThR, thalamic recipient area. Scale bar is 1 mm. (**E**) Summary of the birthdating performed at early (E4, magenta), intermediate (E6, gold), or late (E8, cyan) neurogenic time points. Two coronal sections are shown, one anterior (top row) and one at posterior levels (bottom row). HT, hypothalamus; NPall, nidopallium; PTh, prethalamus. Scale bars are 1 mm. (**F**) Pseudoimage made by the merge of images from three different animals, showing the distribution of pallial cells according to birth time. LPall, lateral pallium; MedNPall, medial nidopallium. Scale bar is 1 mm. (**G** to **I**) Quantitative analysis of the neurogenesis of DVR circuit cells. Shown in (G) is a bar graph representation of the temporal neurogenic construction of the neurons of the different DVR circuit roles after data normalization in order to represent which percentage of the neurogenesis (out of the total 100%, which takes place from E4 to E9 in chick) occurs at early, intermediate, or late time points. Shown in (H) is a bar graph representation of the distribution of DVR circuit neurons generated at each analyzed neurogenic time point. Bars represent mean ± SEM. Dots show individual data (n = 6 chicks per E4 group, n = 7 chicks in E6 APall, n = 8 chicks in EPall and dNPall, n = 6 chicks per E8 group). One-way analysis of variance (ANOVA) followed by all pairwise multiple comparisons by Holm-Sidak post hoc test was performed for E4 and E8; for E6, Kruskall-Wallis one-way ANOVA followed by all pairwise multiple comparisons (Dunn's method) was performed. *p < 0.05; **p < 0.01; ***p < 0.001. Shown in (I) is a statistical comparison of the effect of age on the generation of the cells of each DVR circuit role. Bars represent mean ± SEM. Dots show individual data (n = 6 chicks per E4 group, n = 7 chicks in E6 APall, n = 8 chicks in EPall and dNPall, n = 6 chicks per E8 group). One-way ANOVA followed by all pairwise multiple comparisons by Holm-Sidak post hoc test was performed for APall and EPall; for dNPall, Kruskall-Wallis one-way ANOVA followed by all pairwise multiple comparisons (Dunn's method) was performed. *p < 0.05; ***p < 0.001. (**J**) Summary of the comparative birthdating of mammalian cortical versus avian DVR sensory circuits. The graph depicts the percentage of cells of each circuit role generated at early, intermediate, or late neurogenic time points.

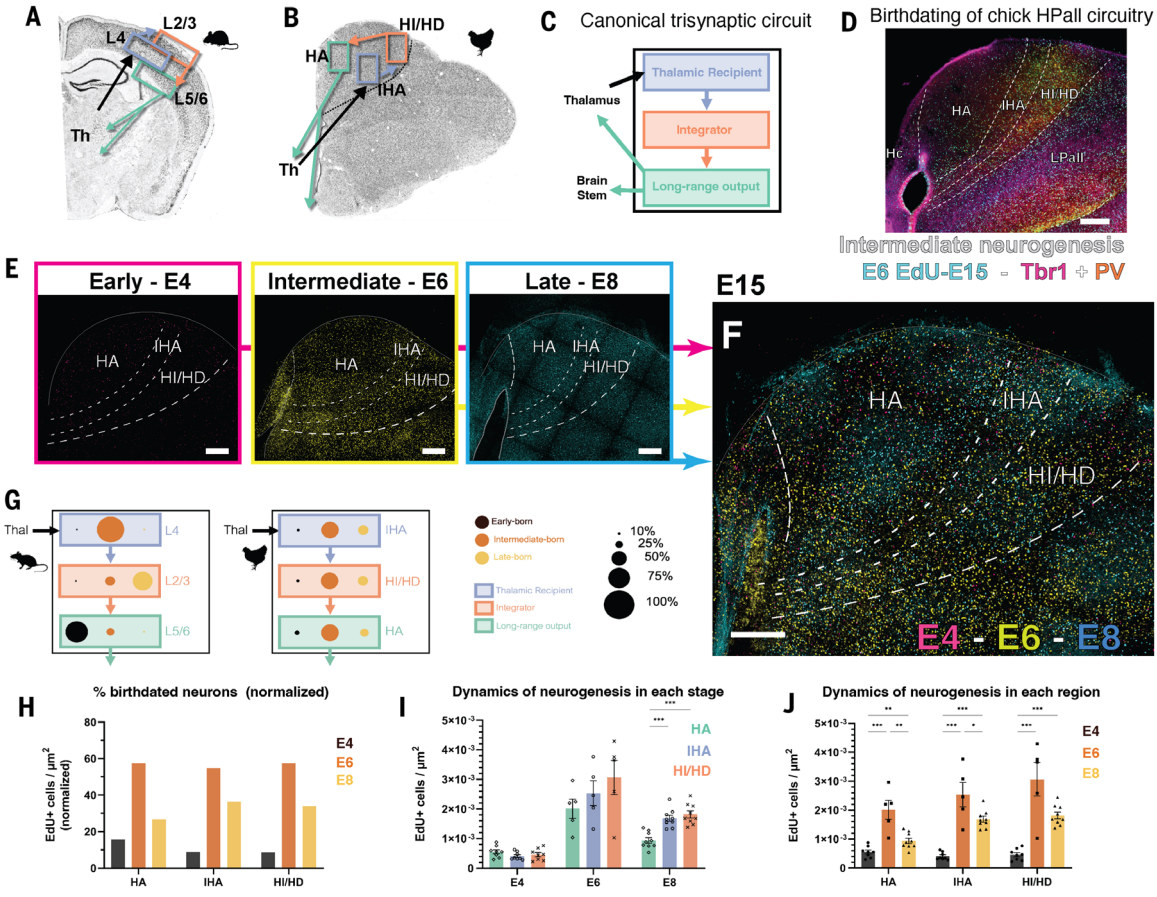

Fig. 2. Neuronal birthdating of the components of the chick hyperpallial sensory circuit. (**A**) Schematic highlighting the connections of the mammalian cortical canonical circuit. Th, thalamus. (**B**) Equivalent schematic depicting the connections of the chick hyperpallial canonical circuit. (**C**) Scheme of the basic cell type organization in the trisynaptic circuit of amniotes. (**D**) Example of coronal section of the chick telencephalon in a typical experiment, where EdU is labeled (cyan) along with two markers by immunohistochemistry, PV (orange) and Tbr1 (magenta). Hc, hippocampus, Scale bar is 250 µm. (**E**) Summary of the birthdating performed at early (E4, magenta), intermediate (E6, gold), or late (E8, cyan) neurogenic time points. Scale bars are 250 µm. (**F**) Pseudoimage made by the merge of images from three different animals, showing the distribution of pallial cells according to birth time. Scale bar is 250 µm. (**G**) Summary of the comparative birthdating of mammalian cortical versus avian hyperpallial sensory circuits. The graph depicts the percentage of cells of each circuit station generated at early, intermediate, or late neurogenic time points. (**H** to **J**) Quantitative analysis of the hyperpallial circuit neurogenesis. Shown in (H) is a bar graph representation of the temporal neurogenic construction of the neurons of the different hyperpallial circuit roles after data normalization in order to represent which percentage of the neurogenesis (out of the total 100%, which takes place from E4 to E9 in chick) occurs at early, intermediate, or late time points. Shown in (I) is a statistical comparison of the distribution of hyperpallial circuit neurons generated at each analyzed neurogenic time point. Bars represent mean ± SEM. Dots show individual data (n = 8 chicks per E4 group, n = 5 chicks per E6 group, n = 9 chicks per E8 group). One-way ANOVA followed by all pairwise multiple comparisons by Holm-Sidak post hoc test was performed. ****$p < 0.001$. Shown in (J) is a bar graph representation of the effect of age in the generation of the cells of each hyperpallial circuit roles. Bars represent mean ± SEM. Dots show individual data (n = 8 chicks per E4 group, n = 5 chicks per E6 group, n = 9 chicks per E8 group). Datasets did not comply with ANOVA assumptions (normality for IHA and HI/HD; and homoscedasticity for HA), so they were logarithmically transformed before the analysis. For all transformed datasets, one-way ANOVA followed by all pairwise multiple comparisons by Holm-Sidak post hoc test was performed. *$p < 0.05$; **$p < 0.01$; ***$p < 0.001$.

pallial areas play defined roles in the trisynaptic circuit: The entopallium (EPall) receives visual sensory input from the thalamus (*26*) and is considered homologous to layer IV (L4) cortical neurons; the neurons in the dorsal nidopallium (dNPall) act as integrators (*14*) and could be homologous to upper L2 and L3 cortical neurons; and those in the arcopallium (APall) project long-range output connections away from the pallium (*27*) in a similar fashion as deep-layer cortical neurons of L5 and L6 (Fig. 1, A and B, although a proportion of deep-layer cortical neurons are intratelencephalic projecting neurons and are, therefore, integrators, as we discuss in the next sections). However, DVR neurons developed following temporal neurogenic instructions different from those present in the developing cortex. Two crucial differences were as follows: First, the earliest-generated neurons act as thalamic recipient neurons within the EPall and the nucleus basalis (BSS; Fig. 1, E to J, and fig. S1), whereas in mouse, other cortical populations are generated earlier to thalamic recipient neurons of L4; and second, the latest-generated neurons of the DVR at the telencephalic level of the EPall do not contribute to sensory processing because they remain in the most medial nidopallium (Fig. 1, E to J, and fig. S1). These results are similar to those previously described (*28*, *29*). In the case of mammals, all cortical neurons contribute to the circuitry, and the latest-generated neurons act as integrators of the circuit in supragranular L2 and L3 (fig. S12).

Beyond timing differences in the formation of the sensory neurons, we also found other

dissimilarities between these two circuits. GABAergic interneurons, which are widely conserved among vertebrate pallia, distribute differently in these circuits. For instance, parvalbumin (PV)–expressing interneurons of the DVR are nearly exclusively located in the thalamic recipient areas (Fig. 1 and figs. S2 and S3), whereas in mammals, these neurons are widely distributed across all cortical layers (*30*, *31*). However, PV expression varies widely over development time and species, and therefore it cannot be trusted in isolation for establishing evolutionary comparisons. Somatostatin (SST)–expressing neurons, on the contrary, are dispersed throughout all regions of the avian circuit (Fig. 1 and fig. S4), whereas they are preferentially confined to deep cortical layers in mammals (*32*).

In addition, other developmental features in charge of building these circuits were different between mammalian cortex and avian DVR. Whereas the glutamatergic component of the neocortex derives from the of the dorsal pallium (DPall) (*33*, *34*), the glutamatergic DVR derives from the ventral pallium (VPall; Fig. 1) (*35*, *36*). This is a distinct discrete region of the embryonic pallium that differs from the DPall in the expression of key TFs (*33*, *35*, *37*), cell lineage, and mature structures derived (in mammals, the VPall mostly generates the pallial amygdala and the pyriform cortex) (*38*). These DPall and VPall early developmental regions are so deeply conserved (*11*, *39*, *40*) that only cell types that arise within the same territory are considered homologous. Thus, the neocortex and DVR likely derive from nonfield homologous progenitor populations, further supporting that those circuits are generated under different developmental programs.

The trisynaptic circuit in the DVR represents the building block of its internal connectivity, but it oversimplifies the true connections. The ventral mesopallium plays a substantial role as integrator in the circuitry by receiving both EPall and dNPall connections and by sending efferents toward the APall (*14*). In our view, the mesopallial component of the circuit has no direct developmental comparison to any neuron of the mouse canonical circuit. The mammalian cortical circuit develops radially, and all neurons derive from the same pallial domain. On the contrary, mesopallial cells do not develop radially with respect to the rest of the nidopallial DVR; they are generated in the lateral pallial germinative zone and their neurons migrate within the limits of the mesopallium (*41*), whereas nidopallial neurons are generated in the ventral pallium and their neurons migrate radially and rostrally within the limits of the nidopallium (*35*). In terms of developmental origin, mesopallial cells have been directly compared with neurons of the claustrum and insular cortex (*41*, *42*), which do not belong to the canonical cortical circuit. And so, we analyzed mesopallial main neurogenic waves separately in order to evaluate its similarities to integrator neurons of the neocortex (fig. S5), considering that this is the role of mesopallial neurons in the avian pallium. The main neurogenic time point of the ventral mesopallium occurs during the intermediate stages, similarly to the other integrator neurons of the dNPall. However, this is different from the late neurogenic time point of mammalian integrator neurons. Moreover, the ventral mesopallium is generated in the lateral pallium, a different developmental area than the rest of the DVR circuit.

The DVR circuits described above mainly represent the visual and somatosensorial circuits in the VPall. We also assessed the sequence of neurogenesis of the auditory Field L in the posterior nidopallium, another sensory circuit (*43*). We found that most of its neurons were generated at late neurogenic time points (fig. S6). This implies that the Field L auditory circuit has a different development than other DVR circuits and the mammalian neocortical circuit. These findings are in agreement with previously described birthdating analysis in dNPall and Field L (*28*, *29*).

We next examined the program of development of the HPall. The glutamatergic neurons of the mammalian neocortex and the avian HPall are all derivatives of the DPall; therefore, the two structures are considered to be field homologous (derived from the same germinal primordium in the brain) (*16*, *17*), and their circuits could more likely be constructed under conserved developmental cues. The ventral limit of the HPall is debated in the literature (*44*), and according to the staining with classical markers at E15 (fig. S7), we adhere to the view of the avian brain consortium nomenclature (*45*), which is also reported in another atlas (*46*). We analyzed the same brains used for the DVR but focused on the neurogenic program of the HPall. In the case of the HPall, the well-known connectivity of the neurons of its columns suggests homologies to neurons of cortical layers (Fig. 2, A and B). Thalamic recipient neurons reside in the intercalated HPall (IHA, similarly to EPall and L4), neurons of the HPall intermediate and densocellulare (HI/HD) act as integrator neurons (as dNPall and L2/3 neurons), and finally, neurons of the HPall apicale (HA) send long-range output connections to extrapallial areas (similarly to APall and L5/L6 neurons) (*47*–*49*). Our analysis shows key differences in the temporal generation of HPall neurons (Fig. 2 and figs. S8 to S11). HPall neurogenesis happened much faster than neocortical neurogenesis. Most HPall neurons were generated quickly during intermediate- and late-neurogenic stages (E6 and E8 stages in chick), and only a minor fraction of them were generated at earlier stages. This late generation is coupled to the reported hyperpallial late maturation of gene expression (*10*). Both E6- and E8-generated HPall neurons settled in all three HPall functional columns (Fig. 2 and figs. S8 to S11). Thus, differently from the mammalian cortex, HPall neurons are not cell fate–determined at the time of generation (fig. S12). We did not identify any cell fate preference correlated to the neurogenic time of HPall neurons (Fig. 2, G to J, and figs. S8 to S11). This is a clear-cut difference from the neocortex, where, instead, a strong correlation between the time when a neuron is generated and its final function within the circuit exists (*23*). Glutamatergic and GABAergic neurons of each HPall column were generated synchronously at the same embryonic stage (figs. S8 to S11), a shared feature between the DVR and the mammalian cortex. Accordingly, although HPall and neocortex are field homologous, their neurons develop following divergent developmental programs.

In addition, the distribution of interneuron types was also different from that of mammalian cortical layers. Most PV-expressing neurons settled in the HI/HD (figs. S7 and S10), a suggested homologous area of the integrator L2 and L3, whereas PV-expressing interneurons widely distribute through all cortical layers in mammals (*30*, *31*).

These data show evidence that the components of the two main high-order sensory circuits in birds, the DVR and HPall, develop following a different program from that known in mammals (Figs. 1J and 2G), thus suggesting that these circuits do not derive from a shared ancestral circuit but instead likely evolved following different developmental programs.

Neurogenic time of the components of gecko pallial sensory circuits

Because birds possess a highly specialized brain in the diapsid taxon (*50*), we further characterized the developmental neurogenesis of sensory circuits in a nonavian diapsid species—the ground Madagascar gecko *Paroedura picta*. This species displays a pallium with fewer specializations than that of birds, thus better resembling the ancestral condition of the amniote group (*51*). The gecko pallium receives and processes thalamic sensory information in two main structures, the DVR (*52*, *53*) and the dorsal cortex (DC) (*54*–*56*).

We identified the DVR and DC as well as the different neurons within them using multiple approaches. First, we used the expression of gene markers such as Tbr1 or Satb2 (Fig. 3A; Satb2 antibody recognizes both Satb2- and Satb1-expressing neurons). In addition, we performed in situ hybridization to detect the expression of known markers for long-range output neurons (*Etv1* and *Sulf2*; Fig. 3, B and C) and thalamic recipient neurons (*Satb1*; Fig. 3, B and E), which are known markers in the mammalian cortex (*57*, *58*) and predicted markers for reptilian pallial cells (*11*, *59*). The expression

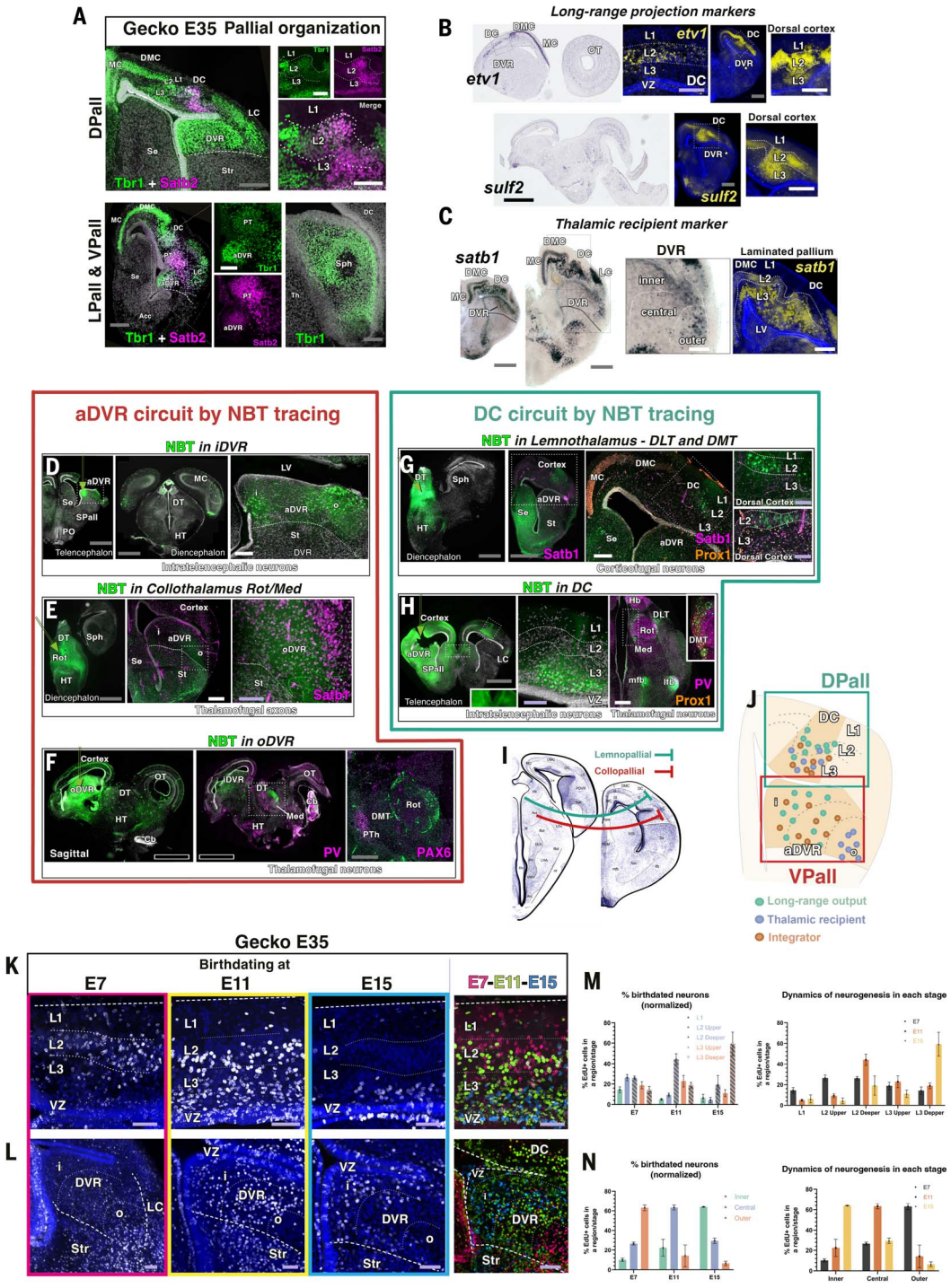

Fig. 3. Neuronal birthdating of the components of the gecko pallial sensory circuit. (**A**) Examples of immunostaining for general pallial markers (Tbr1 in green; SatB2 and SatB1 in magenta) in gecko coronal sections. DAPI (4′,6-diamidino-2-phenylindole) counterstain is in gray. Acc, accumbens nucleus; DMC, dorsomedial cortex; aDVR, anterior DVR; LC, lateral cortex; MC, medial cortex; PT, pallial thickening; Se, septum; Sph, spherical nucleus; Str, striatum; Th, thalamus. Scale bars are 250 μm (gray) and 100 μm (white). (**B**) In situ hybridization against *etv1* and *sulf2* mRNAs in the E35 gecko brain, markers of long-range output neurons in mice. Sagittal and coronal sections are shown. Images on the right show colorimetric staining, pseudotransformed in fluorescent gold staining. DAPI counterstain is in blue. OT, optic tectum; VZ, ventricular zone. Scale bars are 1 mm (black), 250 μm (gray), and 100 μm (white). (**C**) Colorimetric in situ hybridization against *satb1*, marker of thalamic recipient neurons in mouse cortex, in coronal sections of the E35 gecko telencephalon, pesudotransformed in fluorescent gold (images on the right). Satb1 expression is highest at the outer portion of the DVR in the collothalamic pathway and in the deeper layers of the DC (L3 and deep L2). DAPI counterstain is in blue. Scale bars are 250 μm (gray) and 100 μm (white). (**D** to **H**) NBT tracing (green staining) in the gecko pallial circuits at both the aDVR [(D) to (F)] and DC [(G) and (H)] levels. DAPI counterstain is in gray. Representative coronal [(D) to (G)] and sagittal (H) sections depicting the location of those neurons that receive thalamic input, those that project out of the cortex, or those projecting in an intracortical fashion, costained (magenta or orange staining) with antibodies against relevant proteins of the pallium and thalamus. Cb, cerebellum; DLT, dorsolateral thalamic nucleus; DMT, dorsomedial thalamic nucleus; DT, dorsal thalamus; Hb, habenular complex; HT, hypothalamus; I, inner; iDVR, inner DVR; lfb, lateral forebrain bundle; LV, lateral ventricle; Med, nucleus medialis; mfb, medial forebrain bundle; o, outer; PO, preoptic area; PTh, prethalamus; Rot, rotundus nucleus. Scale bars are 1 mm (black), 250 μm (gray), 100 μm (white), and 50 μm (light purple). (**I**) Schematic of two coronal sections of the gecko brain depicting the two main communications of the thalamopallial pathway: the lemnothalamic pathway reaching the DC (teal) and the collopallial pathway reaching the aDVR (magenta) as described from NBT tracing. (**J**) Schematic depicting a coronal section of the chick telencephalon with the location of neurons of pallial circuits. (**K** and **M**) Birthdating of the DC neurons at three neurogenic stages. DAPI counterstain is in blue. Shown in (K) are images of the EdU labeling. On the right is a pseudoimage made by the merge of images from three different animals, showing the distribution of DC cells according to birth time. Shown in (M) is a semiquantification analysis of the birthdating in the DC. No statistical analyses were performed because of the low number of gecko embryos obtained (three at early birthdating, three at intermediate birthdating, and two at late birthdating). (**L** and **N**) Birthdating of the DVR neurons at three neurogenic stages. Shown in (L) are images of the EdU labeling. On the right is a pseudoimage made by the merge of images from three different animals, showing the distribution of DVR cells according to birth time. Shown in (N) is a semiquantification analysis of the birthdating in DVR. No statistical analyses were performed because of the low number of gecko embryos obtained (three at early birthdating, three at intermediate birthdating, and two at late birthdating).

of these genes suggested the locations of different neuronal types in the pallium. To test this hypothesis, we performed axonal tracing using neurobiotin (NBT) electroporation, which revealed mostly retrograde tracing, but some anterograde tracing, too (Fig. 3, D to I), and which depicted a pattern of connections equivalent to that in other reptiles [reviewed in (*50*)]. NBT tracing in the inner part of the DVR (iDVR) revealed retrograde traced neurons in the outer portion of the DVR (oDVR), suggesting that iDVR neurons project locally within the DVR (Fig. 3D). No extratelencephalic labeling was detected. Tracing from the collothalamic nuclei revealed axons reaching the oDVR, in close proximity to Satb1-expressing neurons (Fig. 3E). When the NBT electroporation was targeted to the oDVR, the recipient of thalamic axons, we consequently found retrogradely labeled neurons in the rotundus and medialis nuclei of the thalamus (Fig. 3, F and I). Our tracing of the DVR neurons is in line with previous literature on the axonal connectivity of the DVR in *Gekko gecko* and other lizard species (*52*, *53*). Analysis of the connectivity of DC neurons after NBT retrogradely tracing from lemnothalamic nuclei showed that corticothalamic projecting neurons were located in L2 of the DC (Fig. 3G). These long-range output neurons in L2 were located above Satb1-expressing neurons of L3 (Fig. 3G), which suggests that thalamic recipient neurons are located in this deep layer (Fig. 3G). When the NBT tracing was targeted to the DC, intercortical projecting neurons were labeled contralaterally in L3 (Fig. 3H). The connectivity described here in the gecko DC matches previous findings in other lepidosaurian lizards (*54*–*56*). Altogether, we identified the location of the main types of gecko pallial neurons (Fig. 3J) and focused our attention on the crucial populations for evolutionary comparison: In the DC, long-range output cells settle in L2, in line with available literature. Precisely, it has been shown that turtle DC neurons with higher similarity to cortical long-range output neurons are located in the upper half of L2 (*11*). As for the DVR circuitry, we identified that the thalamic recipient neurons were located in the outer region of the DVR, according to *Satb1* expression and to its communication with the thalamus found with NBT.

We then performed equivalent birthdating experiments to those we performed in chick. We injected EdU at three different time points during the neurogenic period of the gecko pallium (E7 to E15) in order to reveal the temporal neurogenesis of the reptilian sensory neurons (Fig. 3, K and M). The developmental program that gives rise to the DVR, in the VPall, followed a clear outside-first–inside-last gradient of neurogenesis (Fig. 3, L and N). Early born (E7) DVR neurons of the gecko were located in the outermost region of the DVR, deep beneath the lateral cortex. At intermediate stages (E11), newborn neurons tended to be located in the central portions of the DVR. Finally, the latest-generated neurons (E15) hardly migrated away from the ventricular surroundings and were located in the innermost DVR region. An equivalent outside-in gradient of neurogenesis also led to the formation of the DC, in the DPall, although it was not as sharply clear as in the DVR (Fig. 3, K and M). Early generated neurons (E7) in the dorsal cortex were mostly located in the compact, cell-dense L2. At intermediate stages (E11), newborn neurons settle in L3 and the deep stratum of L2, suggesting that the earliest neurons were located in the upper half of L2. The latest-generated neurons barely separated away from their original site at the ventricular zone and were located in the deepest stratum of L3.

This sequential neurogenesis verified that, akin to chicks but in stark contrast to the mouse neocortex, the initial neurons generated in the VPall sensory circuit in geckos were thalamic recipient neurons. The neurogenic progression observed in the DVR appears to be conserved in sauropsids, deviating from the pattern observed in mammals. Regarding the DPall sensory circuit, it is probable that geckos and mammals exhibit shared neurogenic characteristics. In both taxa, the long-range output neurons emerge as the first neurons in the circuit, diverging from the pattern observed in any avian pallial circuit. These data support the notion that pallial circuits develop differently across amniotes, which suggests evolutionary diversity.

Single-cell RNA sequencing of early born pallial populations

To clarify that the glutamatergic neurons in pallial amniote circuits are not conserved homologous cells and to demonstrate that the developmental differences extend beyond a mere switch in the sequence of cell type formation or their specific pallial origin, we analyzed their transcriptional signatures and developmental trajectories. We used our original BirthSeq method (*60*) to isolate and analyze birthdated cells days after their generation time. This method allowed us to compare those chick and mouse pallial neurons that were generated at equivalent neurogenic time points (see supplementary materials and methods). By applying BirthSeq, we performed single-cell RNA sequencing (scRNA-seq) only on cells generated early during the formation of the pallial circuits, both in chick (cells born during the E4 to E6 period; Fig. 4A) and in mouse (cells born during E12 to E14; Fig. 4D). We focused on the earliest-born pallial neurons because these were shown to play divergent roles in the sensory circuit of the two species (Figs. 1 and 2).

BirthSeq provided us with two datasets of maturing cells (11 days after EdU administration) enriched in neurons generated early in pallial development [Fig. 4 and figs. S13 to S16, as also detailed in (*60*)]. The chick pallium dataset comprised 3123 neurons distributed in eight clusters (Fig. 4, A to C, and figs. S13 and S14). The mouse pallium dataset comprised 3634 neurons distributed in nine clusters [Fig. 4, D to F, fig. S15, and described in (*60*)]. Datasets for each species comprised both glutamatergic neurons generated within the pallium and GABAergic interneurons that migrated tangentially from the subpallium (SPall; *34*, *60*–*62*). BirthSeq did not allow us to directly link the identity of the sequenced cells with their projection profile, and each cell cluster could potentially comprise several cell types with different connectivity patterns. However, this is unlikely according to the current literature (*63*). We compared all cells between both species, regardless of their connectivity pattern, which was only revealed by further research. In this regard, when comparing the differentially expressed (DE) genes of these neurons, we observed that many of them were not common among the glutamatergic clusters of the two species, whereas there were more similarities in the GABAergic clusters [Fig. 4, C and F, and figs. S13 to S15 heatmaps and (*60*)]. For instance, mouse glutamatergic clusters (*Neurod6*, *Slc17a6*) were identified by the expression of *Sox11*, *Id2*, *Pcp4*, and *Mef2c* genes (*60*), whereas in the case of the chick glutamatergic cluster, the DE genes were *NRN1*, *NRP2*, *PPP1R17*, *TENM3*, or *SATB2*. In the case of GABAergic clusters (*Nrxn3*, *Gad*), some clusters shared the expression of interneuron subtypes such as *SST*, *ZFHX3*, *ADARB2*, or *MEIS2* (*60*). To compare cells from both species, we integrated the two datasets to identify cell similarities (Fig. 4G). GABAergic interneurons appeared largely similar after principal components analysis clustering and formed mixed clusters at different resolutions, which pointed to transcriptomic similarities. Conversely, glutamatergic neurons exhibited a more dispersed, species-specific organization. A notable example is the Cajal-Retzius cells (msGLUT-05, characterized by *Reln* and *Lhx1* expression), which are the first cells generated in the cortical neuroepithelium (*64*, *65*) and which were specific to the mouse dataset. The integrated dataset clustering showed that, among the six glutamatergic clusters, four were considered species specific (two chick specific and two mouse specific, with more than 85% cells coming from the main species), whereas none of the four GABAergic clusters included such a majority of cells from one single species (Fig. 4H). The broader transcriptomic similarity of GABAergic neurons was then confirmed by the correlation of gene specificity indexes [GSIs; (*11*)] (Fig. 4I). When comparing the TFs expressed in the two datasets—namely the genes more involved in cellular specification during development—the largest correlations (up to 0.86) were found among GABAergic cells. Transcriptomic correlation was larger between pairs of clusters, which suggests transcriptomic equivalence in a one-to-one cell-type

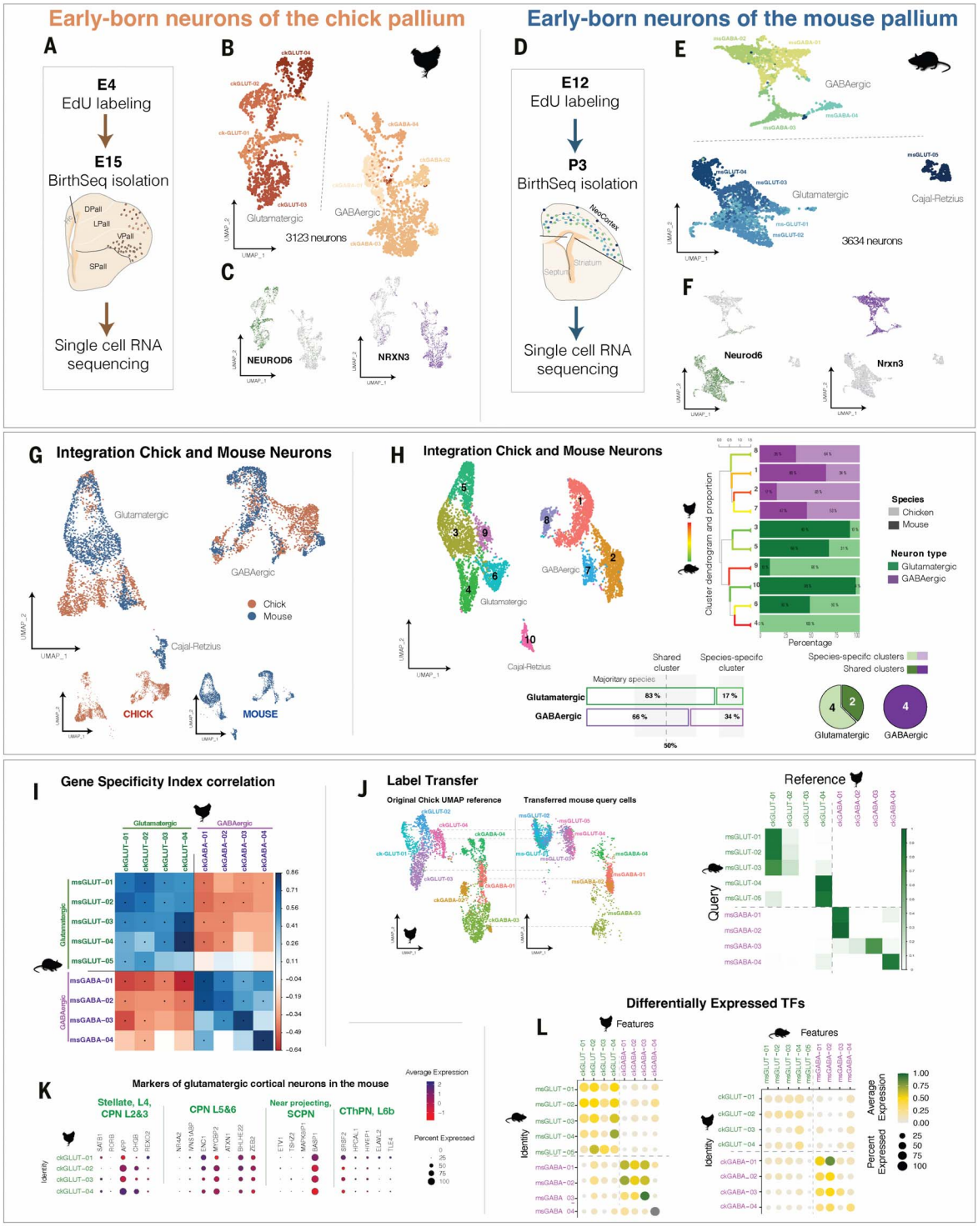

Fig. 4. Transcriptomic comparison of chick and mouse early born pallial neurons. (**A** and **D**) Schematic depicting the extraction and analysis of early born neurons in the maturing pallium of chick (3123 neurons, obtained from three embryos) (A) and mouse (3634 neurons, obtained from three pups) (D). Hc, hippocampus. (**B** and **E**) Uniform manifold approximation and projection (UMAP) graph of the main types of chick (B) or mouse (E) early born pallial neurons. (**C** and **F**) Gene expression UMAP graphs of two key markers for glutamatergic (*NEUROD6*) or GABAergic (*NRXN3*) neurons in chick (C) or mouse (F). (**G**) UMAP graph of the Seurat integration merging the two species datasets with equivalent cell number (3123 cells per species, 6246 cells in total). (**H**) Integrated UMAP clustering. On the right is the proportion of each species cells to the integrated clusters. At the bottom left is the average proportion of neurons from each species in either glutamatergic or GABAergic clusters. At the bottom right is the proportion of clusters considered as species-enriched or shared by both species. (**I**) Correlogram of gene specificity indexes between pairs of clusters of the two species. (**J**) Label transfer analysis of mouse cells onto the chick annotated reference UMAP. On the right is the proportion of cells from a mouse cluster that were assigned to a given chick cluster. (**K**) Gene expression DotPlots of key markers for glutamatergic cortical neurons (*58*) for each chicken glutamatergic cell type. (**L**) Percentage of module expression for each cell type (Top4 Marker Genes) on the other species cell types (left, mouse modules; right, chicken modules).

fashion. However, only one chick glutamatergic cluster (ckGLUT-04) was found to be similar to two mouse clusters (msGLUT-03 and -04). No other cell type–to–cell type equivalence was identified. The general GSI similarities between glutamatergic neurons seemed more related to the transcriptional profile leading to the glutamatergic phenotype than to the actual transcriptome involved in specific cell type differentiation. We tested this possibility by comparing the expression of each cluster of DE genes, which tend to play roles in the specification of cell types (Fig. 4L). We generated modules comprising the most DE genes, from either the whole sequenced transcriptome or only from the TF gene family, and analyzed the average expression of these modules in the cell clusters of the opposite species. In the modules comprising the five most differentially expressed TFs for each cluster (Fig. 4L), GABAergic cells seemed to be more similar at the cell type level, regardless of the original species used for defining the module. Conversely, glutamatergic cells only shared a background similarity, especially when mouse clusters were used to define the module of expression. Of the glutamatergic clusters, the ckGLUT-04 cluster (*SATB2*, *MEF2C*, *CCK*, *CRHR2*; fig. S13) was the most similar to a mouse cluster (msGLUT-04, *Mef2c*, *Ptprk*, *Arpp21*, *Satb2*; fig. S15) between the glutamatergic clusters. This mouse cluster likely corresponded to intratelencephalic cortical neurons (*28*), which are abundant in upper layers but also exist in deeper layers.

We then performed label transfer analysis (*6*). Each cell from a dataset was tested to determine to which cell cluster from the other species dataset it was transcriptionally more similar. This test also confirmed that the similarity between early born GABAergic neurons was greater than the similarity between early born glutamatergic neurons (Fig. 4J). Comparisons by canonical correlation analysis (CCA) integration (*66*, *67*) and single-cell regulatory network inference and clustering (SCENIC) analysis (*68*) of regulatory networks also showed greater transcriptomic and TF similarities in the GABAergic lineage (figs. S15 and S16). Although CCA integration depicted similarities between glutamatergic cells, this more coercive methodology should be interpreted with caution. In the CCA integration, mouse Cajal-Retzius cells and several different glutamatergic and GABAergic clusters of the chick pallium (cluster GLUT/GABA7 in fig. S16) are mistakenly clustered together. Altogether, these analyses support the notion that among taxa, the different developmental program of early born glutamatergic neurons is the blueprint of divergent differentiation programs for these cells, as reflected by their different transcriptomes. On the contrary, GABAergic cells are likely generated by a more conserved development program, as reflected by the higher conservation at the transcriptional level.

To support this possibility, we also checked whether chick early born glutamatergic neurons expressed the typical molecular signatures of either upper-layer or deeper-layer neurons of the mouse cortex (*58*). We identified that some typical TFs and genes were expressed by one or more chick clusters, but the combination of those TFs typical of a cortical cell type was not found in any chick cluster (Fig. 4K). This implies that mouse and chick glutamatergic neurons are not parallel cell types, and their diverged developmental sequence reflects a major deviation of developmental programs leading to different neurons. Thus, early born chick glutamatergic neurons exhibit profound differences from their mouse counterparts across multiple levels of comparison. Furthermore, these chick neurons share no substantial similarity with either upper- or deeper-layer cortical neurons in mammals. This distinct divergence strongly suggests that their transcriptional signature has evolved independently from both mammalian types, underscoring a separate evolutionary trajectory.

To understand how early born glutamatergic neurons diverged in their maturing transcriptome, we analyzed the transcriptomic developmental trajectories of these neurons. We birthdated early cells (E4 in chick and E12 in mouse) and applied BirthSeq 2 days after EdU administration. We then sequenced birthdated cells comprising early differentiating neuroblasts and progenitors at intermediate pallial neurogenesis (E6 in chick and E14 in mouse) (Figs. 5 and figs. S17 to S20). We performed a comparison of both species' datasets: cell cluster identification, integration of datasets, GSI correlation, DE gene module analysis, and label transfer. These experiments brought up three main results. First, among the various cell types sequenced, the strongest similarities were observed between the neural stem cells of both species, particularly the pallial RGCs, which displayed a high degree of transcriptomic similarity (Fig. 5). Although a population of mouse intermediate precursor cells (IPCs) enriched in *Eomes* expression was clearly identified, a comparable population in chicks remained elusive (*19*). No transcriptomic equivalent of IPCs was detected in the chick dataset, as indicated by the absence of merged IPCs in the integrated datasets (Fig. 5G). However, when integration was performed without the typical cell cycle correction (fig. S19), the ckGLUT-01e cluster included a subset of cells that displayed some mouse IPC characteristics. Additionally, we observed cellular divisions away from the ventricular surface, which are indicative of a germinative subventricular zone in the developing chick pallium (fig. S19G). These findings suggest the presence of IPCs with a previously uncharacterized transcriptomic profile in the chick pallium, although their contribution to pallial neurogenesis appears substantially more limited than that of mammalian IPCs, as evidenced by the relatively low abundance of chick IPCs. Second, GABAergic cells showed the largest similarities between specific neuronal types also during their differentiation progress (Fig. 5, G to K). Third, and finally, we observed that some transcriptomic dissimilarities between glutamatergic cells are determined early after birth date. Glutamatergic cells from both species showed transcriptomic similarities related to the differentiation of main glutamatergic type (*TBR1*, *SLC17A6*, *NEUROD* genes) and a minor equivalence of specific cell types. As described above, these divergences are more pronounced between the maturing neuron datasets. This implies that the transcriptomic divergence is likely determined very early in their development. In conclusion, our scRNA-seq analysis of early born neurons of the pallium showed substantial disparities between the transcriptomic programs of GABAergic and glutamatergic neurons of both species. These programs were mainly divergent between the glutamatergic populations, whereas they were deeply conserved between GABAergic neurons.

Distribution of early born chick pallial neurons

The locations of specific transcriptional cell types within the chick pallium remain largely unknown. To investigate and describe the distribution of these distinct cell types, we conducted in situ sequencing (ISS) for genes that identify early born neuronal clusters (Fig. 5 and figs. S21 to S23). Using 84 genes selected from our scRNA-seq analysis, we examined their expression at a cellular level in coronal sections of three E15 chick brains. Many of these genes were expressed exclusively in different telencephalic sectors, enabling the identification of various pallial territories and circuit stations (Fig. 6A and fig. S21). A total of 911,495 cells were sequenced and analyzed. By comparing ISS reads to clusters identified through scRNA-seq, we detected 660,117 neurons in the tissue that matched our scRNA-seq clusters (Fig. 6B). This correspondence was determined by the expression of significant genes in the ISS data (Fig. 6, B and C). Glutamatergic neurons were found to be distributed in four clusters across different pallial regions, exhibiting distinct gene expression patterns and functions within the pallial circuitry (Fig. 6, D and E, and fig. S23). GABAergic interneurons also displayed differential distribution among four neuronal clusters, with some spanning the entire pallium and others being more restricted to specific regions (Fig. 6, D and F, and fig. S24). The distribution identified through this probabilistic cell typing reflects that our scRNA-seq clusters correspond to major types of developmental neurons, but not all of those neurons were early born.

To identify the early born neurons among these clusters, we used Neurogenes-ISS, a combination of ISS and EdU birthdating (*60*). This analysis provided information on the location

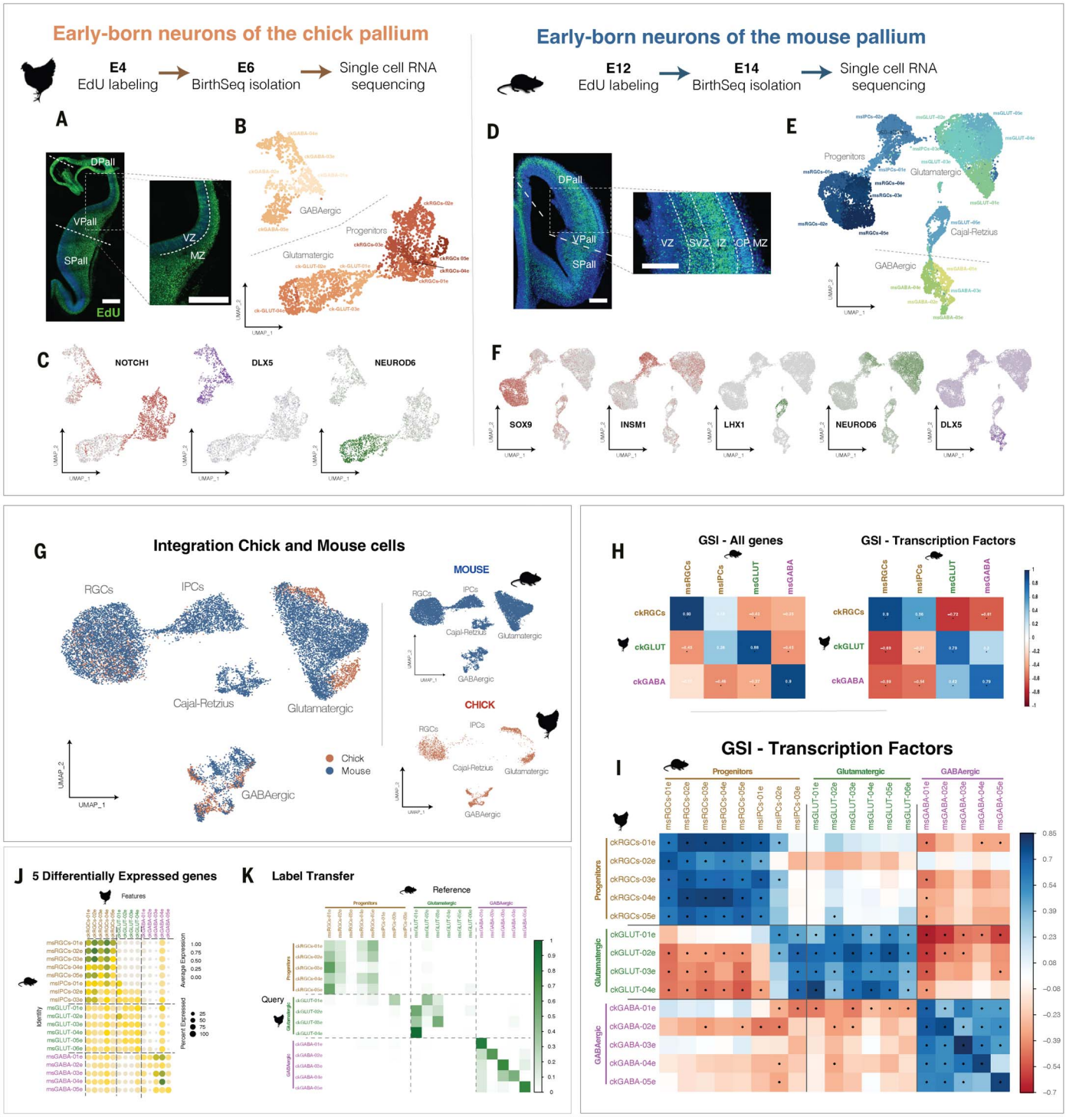

Fig. 5. Transcriptomic comparison of early born neurons and progenitors between chick and mouse. (**A** to **F**) BirthSeq isolation of early born populations 2 days after EdU labeling in chick [(A) to (C)] and mouse [(D) to (F)]. Shown in (A) and (D) is EdU staining of chick and mouse pallia at the moment of cell isolation. CP, cortical plate; IZ, intermediate zone; MZ, marginal zone; VZ, ventricular zone. DAPI counterstain is in blue. Scale bars are 100 μm. Shown in (B) and (E) is a UMAP graph of the main types of chick (3131 cells, obtained from five embryos) (B) or mouse (13,630 cells, obtained from six embryos) (E) early born pallial populations. Shown in (C) and (F) are gene expression UMAP graphs of several key markers for radial glial cells (*NOTCH1*), intermediate precursor cells (*INSM1*), glutamatergic neurons (*NEUROD6*), Cajal-Retzius cells (*LHX1*), or GABAergic (*DLX5*) neurons in chick (C) or mouse (F). (**G**) UMAP graph of the Seurat integration merging the two species datasets (randomly sampled to analyze equivalent cell numbers: 3131 cells per species, 6262 cells in total). (**H**) Correlogram of gene specificity indexes between pairs of main cell types of the two species. (**I**) Correlograms of gene specificity indexes between pairs of clusters of the two species, considering TFs only in the comparison. (**J**) Percentage of module expression for each cell type (Top5 Marker Genes) on the other species cell types. (**K**) Label transfer analysis of chick cells onto the mouse annotated reference. The graph depicts the proportion of cells from a chick cluster that were assigned to a given mouse cluster.

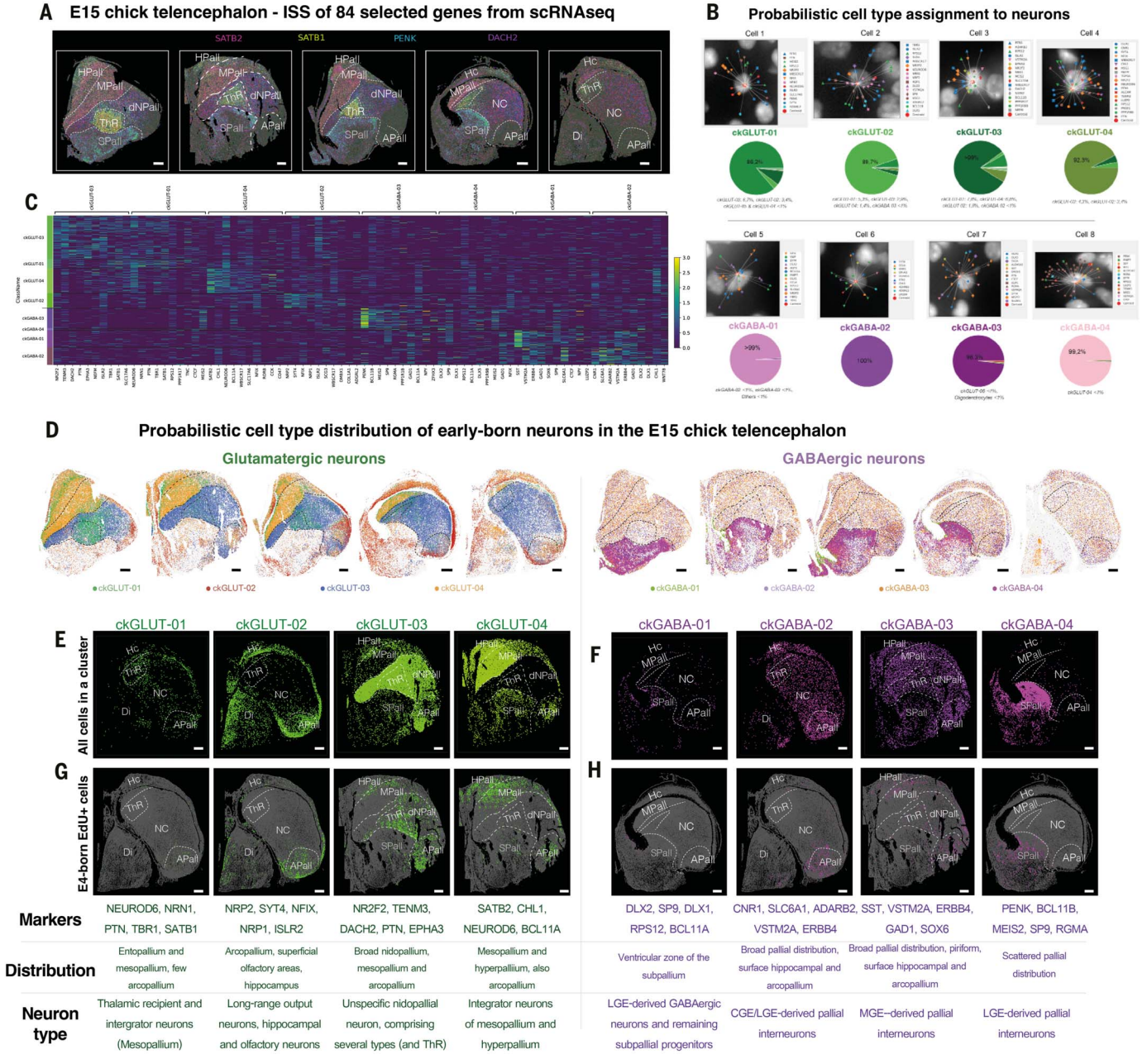

Fig. 6. Identification of early born neurons of the chick pallium by ISS. (**A**) Expression maps of four informative markers, chosen from a panel of 84 ISS genes. Di, diencephalon; Hc, hippocampus; MPall, mesopallium; NC, nidopallium caudale; ThR, thalamic recipient area. Scale bars are 500 μm. (**B**) Examples of in situ probabilistic cell type assignment for the neuronal clusters: For each cell (identified using DAPI signal, in gray), a map of its associated transcripts was built, taking into account the probability of gene coexpression derived from scRNA-seq data (images). Based on its expression profile, each cell was then assigned a probability of belonging to each one of the scRNA-seq clusters (pie charts). (**C**) Heatmap comparison of the gene expression profiles, as detected by informative genes in ISS, of the different cell clusters. (**D**) Anatomical distribution of the glutamatergic and GABAergic neuronal subpopulations. The left panel shows the distribution of glutamatergic neuron types. Scale bars are 500 μm. (**E** to **H**) Joint birthdating and transcriptional profiling of selected cell clusters: Glutamatergic (E) and GABAergic (F) neuronal subclass distributions are shown on two of the samples, together with a description of their characteristic markers, anatomical distributions, and functional annotations (table). Of each neuron subclass, the EdU-positive cells can be extracted and plotted separately [(G) and (H)], allowing analysis of the distribution, across neuron types, of the birthdated cells. This allows one to visually inspect the relationship between birth date and cell identity. Analyzed sections were obtained from three different embryos.

of early born neurons, which usually correlates with their connectivity patterns as described earlier. A fraction of the identified neurons within these clusters (12.3%) were EdU-positive, indicating that their generation occurred shortly after EdU administration at E4. The proportion varied across clusters (from 17.2% for ckGLUT-02 to 5% for ckGABA-04). Neurogenes-ISS facilitated the precise localization of early born neurons, which, along with their known birthdate and transcriptomic identity (Fig. 6, G and H, and figs. S22 and S23), indirectly allowed us to describe their connectional role in the circuit. The distribution of early born neurons ckGLUT-01 to ckGLUT-03 aligned with expectations within

the circuit (EPall, APall), as well as within other pallial territories, such as the hippocampal and parahippocampal areas, the nidopallium caudale, and the mesopallium (fig. S22). Early born neurons in cluster ckGLUT-04, which showed similarity to those in msGLUT-04 (Fig. 4 and fig. S22), were primarily identified as mesopallial cells, and thus, according to the literature, they situated outside the canonical circuit (*4*, *69*). These neurons were indeed predominantly located in the mesopallium and HPall, with some sparsely distributed across parahippocampal regions and the APall.

To compare early born neurons between species, we performed equivalent Neurogenes-ISS labeling of E12-generated mouse cortical neurons (*60*). In addition, this analysis provided insights into the specific projection pattern of specific neuronal clusters. Most early born cortical neurons settle in the deeper layers and lateral areas of the cortices, becoming corticothalamic, deep intratelencephalic neurons, together with insular cortical, claustral, and piriform cortical neurons (figs. S15A and S24). Cajal-Retzius cells and several deep-layer cortical glutamatergic clusters exhibited no transcriptomic similarity to any chick glutamatergic cells (Fig. 4), underscoring a fundamental difference in their transcriptional programs. Furthermore, within all glutamatergic clusters, only the integrator neurons of cluster msGLUT-04 showed any transcriptomic overlap with a chick glutamatergic cluster. These integrator neurons are primarily located in the deep layers of the cortex and the claustro-insular area (fig. S24N), and this singular overlap was independently validated through whole-pallium single-cell transcriptomic comparisons (*70*).

Early born chick GABAergic neurons exhibited a preference for subpallial territories but were also widely distributed throughout the pallial territories (fig. S24). Early born GABAergic PV-expressing neurons in the EPall, primarily generated at E4 in chick (Fig. 1 and fig. S3), were absent in our ISS analysis, possibly due to their absence in our initial scRNA-seq dataset.

Our analysis of the transcriptomics and distribution of early born neurons in the pallium confirmed their expected presence across various pallial regions. Within the circuit regions, glutamatergic neurons were identified as thalamic recipient neurons and long-range output neurons, whereas outside the circuit, they belonged to integrator classes located in other pallial territories, such as the hippocampal, mesopallial, and olfactory areas.

These results reveal fundamental differences between early born neurons in the chick and mouse pallium, spanning developmental, transcriptomic, and distributional dimensions. Despite originating from homologous RGCs, these neurons follow divergent developmental programs in each species, ultimately forming neuronal assemblies in nonequivalent stations of the pallial circuitry. This divergence underscores the distinct evolutionary trajectories that shape pallial architecture in birds and mammals.

Circuit analogy emerges from different neurogenic programs

Although mouse and chick pallial circuits have different development, they supersede similar sensory processes (*71*). We used mathematical modeling to elucidate the possible principles for a potential functional convergence. Each developing pallial circuit consists of a population of neurons electrically coupled mostly by immature synapses and volume signaling (*72*). Although preferential connection may exist, cell coupling within and between individual pallial circuits is mostly diffuse (*73*–*75*). We thus hypothesized that embryonic pallial wiring could be described by a random block-structured adjacency matrix J whose blocks describe specific pallial regions and connections (Figs. 7, A and D). In this framework, a neuron's activity is modeled by a smooth saturating nonlinearity of the sum of the activity of surrounding cells weighted by the connectivity in J (data S2)

In our model, we grew pallial circuits by progressively increasing the size of our matrix blocks, adding neurons at fixed time stamps based on the neurogenesis rates inferred from our data (Fig. 7, B and E). The functional readout of this process is the emergence of scant oscillations and chaotic activity reminiscent of the spontaneous activity in developing pallial areas that is observed experimentally (*76*) and that is reflected by the growth of the disk of the J eigenvalue spectrum beyond a value of one (Fig. 7, C and F). Despite the divergent neurogenic programs and structural differences, analogous values of coupling strength can be found in both mice and chicks, resulting in the growth of the eigenvalue disk and in the emergence of similar spontaneous activity (Fig. 7G). This in turn suggests that neurogenesis programs in the avian and mammalian brain may have converged by evolutionary constraints for adaptation to equivalent functions.

To test this hypothesis, we looked at the spectral energy S of the graph associated with the growing matrix J (*77*). Such energy increases with J randomness and is thus informative with respect to the structure of developing pallial circuits. As we permute the three neurogenic programs among the pallial regions, we found that both avian and mammalian circuits evolved to maximize S (Fig. 7, H and I). The scaling of S by neurogenesis indicates that an initial diverging trend between avian and mammalian different neurogenic programs turns into converging by birth, possibly through differential amplification of telencephalic signaling centers that are shared in both taxa (Fig. 7J). This again suggests that avian and mammalian pallial circuits converged to respond to analogous structural and functional requirements rather than being homologous.

Discussion

For decades, there has been a heated debate around identifying homologies between the mammalian-specific neocortex and that of other vertebrates. Various studies suggest the existence of such a homology, based either on gene expression patterns observed in embryonic brains (*16*, *17*) or on neuronal connectivity patterns (*14*, *15*) found in adult brains. In this work, we tackled the debate from alternative views, researching the developmental formation of the neurons of the pallial circuitry from neurogenic, transcriptional, and mathematical perspectives. Altogether, we demonstrate that the neurons of the circuits in charge of high-order sensory processing have evolved separately in different vertebrate taxa and have likely converged into equivalent circuits with potential similar functions.

In our analysis, we operated under the assumption that conserved traits must also exhibit equivalence in their developmental programs. Conserved homology, in this context, implies the sharing of a developmental feature that originated from a common ancestor, as discussed in a previous work (*19*). Accordingly, although alternative views regard cells with equivalent transcriptomes as homologous, regardless of their divergent developmental origin (*69*), we rather considered these cells—in the rarely documented occasions—as convergent instead (*19*). In the case of the pallium, our assumption was grounded in the belief that the last common ancestor of amniotes already possessed such a structure (*78*). If the circuits of present-day species were truly conserved and homologous, we would expect them to inherit the same developmental program from topologically conserved regions that were already present in the pallium of the last common ancestor. The topological difference between neocortical and DVR circuits alone might not fully exclude the possibility of their homology, because the evolutionary difference of dorsal and ventral domains is not accepted by all researchers in the field (*44*). Neurogenic timing needed to be considered. In a rare possibility, ventral and dorsal circuits might develop under similar neurogenic rules. This could suggest the existence of a conserved homologous circuit derived from a potentially unified, homogeneous pallium in the last common ancestor. To exclude this possibility, our hypothesis incorporated both the topological origin and the neurogenic timing. This dual consideration strengthens our argument for divergent evolutionary pathways, rather than a simple homologous inheritance, and has already proven valid when applied to other distinct brain territories. Recently, through the utilization of the same birthdating techniques across multiple amniote species, we have discovered that the cerebellar circuitry develops following a tightly conserved chronological sequence of neurogenesis, which is responsible

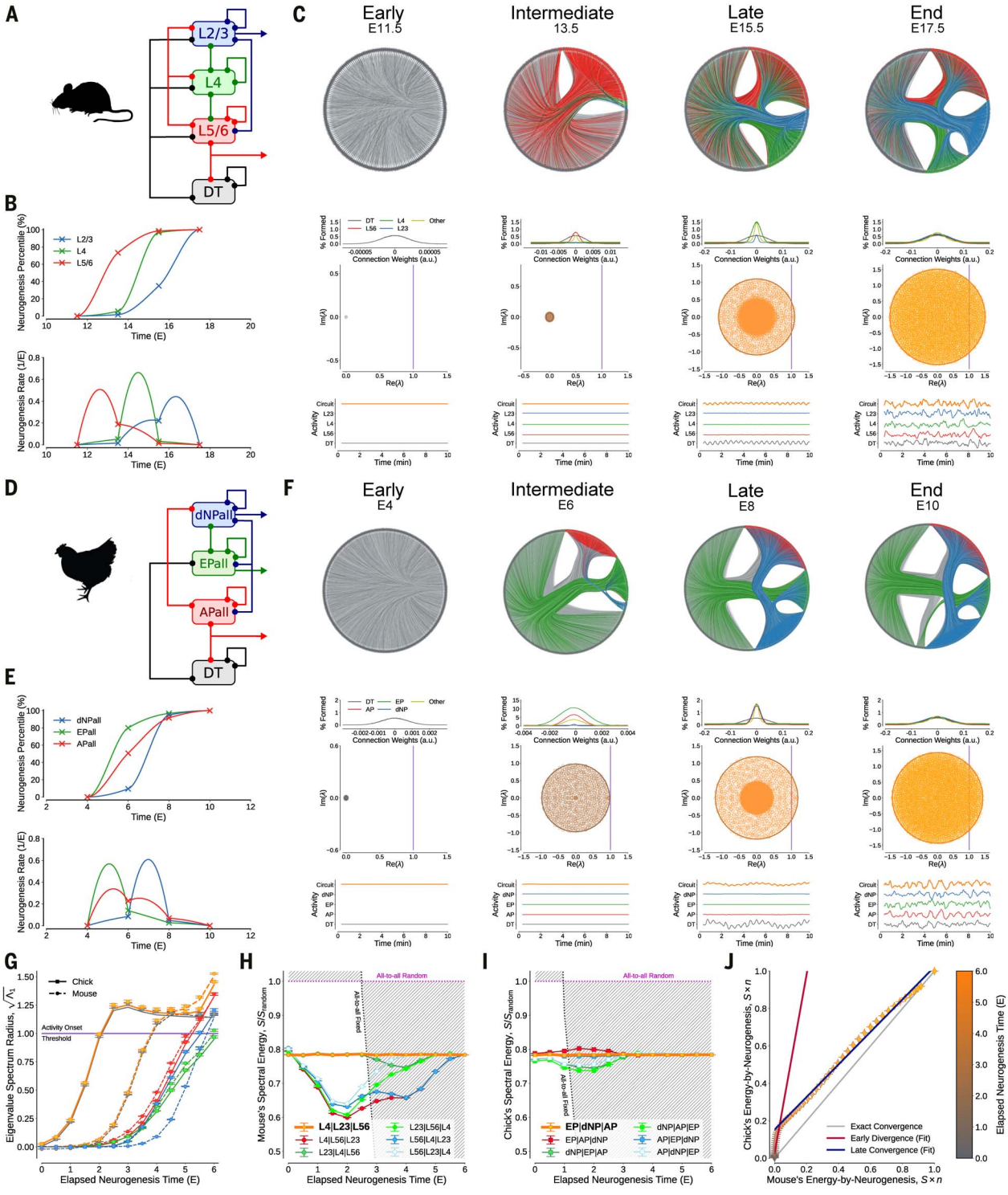

Fig. 7. Mathematical modeling supports structure-function convergence. (**A** to **F**) Mouse (A) and chick (D) pallial circuits and corresponding neurogenesis percentiles (*n*) and completion rates reconstructed from available data [(B) and (E)] (see data S2). DT, dorsal thalamus. Panels (C) and (F) show the simulation of neurogenesis by growth of structured random networks (top graphs), associated weight distribution (top), eigenvalue spectra scatter plots (middle), and representative activity averaged over 10 trials of each pallial area and their ensemble circuit (bottom). AP, arcopallium; a.u., arbitrary units; dNP, dorsal nidopallium; EP, entopallium. (**G**) Evolution of disk radius of the eigenvalue spectrum in thalamopallial relay circuits show similar dynamics independently of neurogenic differences. (**H** and **I**) Spectral energy (*S*) normalized by the energy of the corresponding fully random graph. *S* is generally maximal both in the mouse and chick for the documented neurogenic program but not for any other random permutation of the temporal sequence of the different neurogenic niches. (**J**) Scaling of spectral energy by neurogenesis completion fraction ($S \times n$) reveals late structure-function convergence for avian versus mouse opposed to an initial divergence (blue versus red regression lines).

for the preservation of the cerebellum and its function (*25*). It is this developmental conservation that causes evolutionary conservation. The fact that the pallium develops its circuitry in several different ways strongly supports a nonhomologous character of the amniote pallial circuits.

Other research aimed to identify the sequential development of the pallium of birds, and our results align and expand those findings (*10*, *28*, *29*). Tsai *et al.* (*28*) demonstrated neurogenesis in the chick telencephalon through direct birthdating, but their tools did not analyze cell type or evolution. Suzuki and Hirata (*29*) analyzed mesopallial and hippocampal neurogenesis but excluded the nidopallium, EPall, APall, and HPall. Chen *et al.* (*10*) described gene marker expression in pallial regions, but their data did not directly address the timing of neuron generation, resulting in different findings from ours. The most substantial differences emerge with the Jarvis continuum hypothesis (*10*, *44*, *79*). Chen *et al.*'s data place the mesopallium in their 3° pallium as the last to be generated, whereas our analysis and others (*28*, *29*) show that the mesopallium is generated throughout the neurogenic window. These differences stem from the use of different methodologies. For example, our results and those of Tsai *et al.* (*28*) demonstrate that the earliest pallial neurons formed in the EPall, but Chen *et al.*'s (*10*) gene marker expression of RORB is detected much later in the neurogenesis timeline. Our results on birthdating do not contradict the dorsal and ventral similarities described by the continuum hypothesis (*44*, *79*), which are collaterally supported by our ISS data and were corroborated by snRNA-seq (*70*).

Another crucial factor supporting the divergent developmental nature of these circuits in amniotes is represented by the substantial differences in their progenitor cells. Although pallial RGCs show similarities between the two species, their neurogenic behaviors are different, along with differences in ventral versus dorsal gene expression features (*33*). These differences occur not only at the anatomical level but also at the progenitor cell type level. In mammals, the neocortex is generated in the DPall from multipotent RGCs (*34*, *80*, *81*). However, in birds, the proposed homologous circuit develops in the VPall, which is a distinct pallial territory that predominantly gives rise to the amygdala and olfactory structures in mammals (*35*, *38*). Progenitors in the VPall exhibit transcriptomic differences from those in the DPall, reside in distant regions of the pallium, and are not evolutionary equivalents (*16*).

Neural stem cells in charge of generating the neurons of the circuits also differ with respect to their neurogenic potential. In birds, no single progenitor can generate all the neurons of the DVR circuit. Through electroporations that reveal whole-cell lineage and neuronal migration in chicks, it has been demonstrated that progenitors in the VPall can generate neurons for either the EPall and dNPall, or the APall (*35*, *82*). Therefore, at least two differentially located progenitors are necessary to assemble a functional circuit. This crucially differs from mammals, in which a single RGC is capable of generating each and all the different types of neurons of the cortical circuitry (*34*, *80*, *81*). Additionally, at intermediate stages of pallial neurogenesis in chicks (i.e., around E6), only a small proportion of pallial division happens in the subventricular zone, and its constituent progenitors are not transcriptomically similar to mouse IPCs despite *EOMES* expression. At the equivalent neurogenic time point in mouse cortical neurogenesis (E14 in mouse), IPCs reach their peak population (*83*, *84*). These facts point to differences in the direct and indirect neurogenic pathways, a feature previously referred to as an evolutionary difference between sauropsids and mammals (*85*). Hence, the cellular trajectory of early born pallial neurons in birds differs from that of mammals at all the examined levels, which led to transcriptomic differences in these early born populations. It is likely, though, that IPCs play a more relevant role in avian pallial neurogenesis later in development, as shown in a parallel study after a complete description of the developing cell types in the chick pallium (*70*). This difference in IPCs adds to the observed lack of Cajal-Retzius cells in the pallium of chick [as in (*35*)], suggesting substantial divergences in pallial neurogenesis across amniotes (*19*).

Altogether, our data show an early transcriptomic divergence of glutamatergic cell types between chick and mouse as early as 2 days after their generation. Although our research may be limited by its focus on developmental brains and the specific early stages analyzed using BirthSeq, our findings are likely robust insofar as they fully match equivalent comparisons conducted in mature, adult brains, which included all cell types regardless of their birthdate. The divergence of glutamatergic profiles is further supported by two independent studies that used different methodologies across developing, posthatching, and adult chicks (*70*, *86*). In addition, these studies, along with some of our own ISS data, highlight gene expression similarities at the single-cell level between dorsal and ventral domains, as proposed by the continuum hypothesis (*10*, *44*, *79*). However, these similarities do not indicate a shared developmental trajectory between the two domains nor can they be explained by tangential migration from pallial sources (*35*). Instead, they point to a late convergence of transcriptional profiles (*70*, *86*), reinforcing the idea that divergent developmental programs shape glutamatergic cells.

Our data, as well as those described in (*70*, *86*), suggest a very different scenario for GABAergic cells, that is, a strong conservation of GABAergic pallial neurons. The developmental formation of interneurons follows equivalent sequences of neurogenesis (*10*, *44*, *79*), and transcriptomic analyses also show similar molecular fingerprints of these GABAergic populations. The conservation of GABAergic neurons of the pallium has now been shown to be similar in many different taxa. This conservation was, as stated before, demonstrated by similarities in developmental lineage and transcriptomic profiling. The vertebrate groups tested by transcriptomic comparison have been turtles (*11*), lizards (*59*), amphibians (*40*, *87*), and the distant group of cyclostomes (lampreys), which are jawless vertebrates (*39*). The results on all these species were the same: Homologous populations of GABAergic interneurons are generated in the SPall, migrate tangentially into the pallium, differentiate into interneuron subtypes of equivalent transcriptomic profile, and contribute to the function of pallial circuits. This strong conservation suggests that the modulatory function of GABAergic inhibition plays a fundamental role in pallial sensory circuits, a role that showed a low evolvability, likely due to its relevance. Further investigation into the molecular mechanism and the functional relevance behind this dual evolution of pallial circuits (diversified glutamatergic cells versus conserved GABAergic cells) is warranted.

We speculate that the functional similarities between pallial circuits might be explained by parallel convergent evolution, which limited the formation of the circuits under efficiency restrictions. Many species evolve in the same environment, under the same physical rules, and are driven by the same optimization constraints. As an alternative scenario to the convergence, neurons in these circuits might not have evolved separately to converge into similar circuitries but were already present in the pallium of a common amniote ancestor. In this scenario, the development of the circuit would have been canalized and fixed in evolution (*88*, *89*) owing to its functional importance, although its developmental formation might have been more flexible and divergent. However, we support convergence as the more parsimonious scenario. The developmental changes that we have described likely had a profound impact on both the fate of neurons and the structure and function of the circuits they form. To our knowledge, no other brain circuit presently regarded as homologous exhibits such a marked divergence in foundational features across species. In the unlikely scenario that these circuits were indeed homologous and conserved, we would expect them to share similar functional and developmental characteristics across vertebrate species. Although the existence of trisynaptic circuits in the DPall of teleost fish was initially proposed (*90*, *91*), subsequent research has failed to confirm these findings, and no such circuits have been described in

amphibians. This absence of evidence strongly suggests that these circuits may have originated separately in different vertebrate lineages. Although our methodology cannot definitively rule out homology, the lack of supporting evidence for a conserved origin—coupled with the clear developmental divergence we have observed—strongly argues against the existence of such homology. Ultimately, the pattern of divergence we have documented suggests that the circuits in question have distinct evolutionary origins, and the evidence for homology may simply never be found. Further research, particularly on aspects of circuit formation such as axonal growth and synaptogenesis, would be needed to provide more definitive insights into circuit evolution.

Whether conserved or convergent circuits, the functional similarities among them imply that functionality limits diversity, at all biological levels. This is the case for circuit evolution as well, because circuits may act in similar ways in different species: The shared function of independent circuits limits the diversity of them. We speculate that, following this argument, pallial circuits are more efficient and optimal when arranged in this known fashion (*14*), and brain circuits selected after millions of years of evolution display limited diversity probably because they evolved under the same optimization criteria (*71*). It is likely that convergent evolution sculpted the formation of the components of the sensory circuits in amniote species.

Methods summary

Animal use

All animal experiments were approved by a local ethical review committee and conducted in accordance with personal and project licenses in compliance with the current normative standards of the European Union (Directive 2010/63/EU) and the Spanish Government (Royal Decrees 1201/2005 and 53/2013, Law 32/107). All mice and gecko embryos were from our breeding colonies at Achucarro Basque Center for Neuroscience and the University of the Basque Country (UPV/EHU). Fertilized chick eggs were purchased from Granja Santa Isabel (Spain)

Birthdating

Pregnant mice and sauropsid embryos were injected with EdU at the experimental time according to specific protocols for each species (*25*). Upon completed neurogenesis, neuron migration, and cell differentiation, animals were later sacrificed at the research time following standard anesthesia protocols. The brains were dissected and processed for subsequent experimentation.

Immunohistochemistry and EdU labeling

Brains were fixed with 4% paraformaldehyde (PFA, diluted in 0.1M phosphate buffered saline (PBS), pH 7.3) and sectioned in a vibrating microtome at thicknesses of 50 to 70 μm. Single and double immunohistochemical reactions were performed as described previously (*92*) using a series of commercial primary and secondary antibodies. EdU molecule was later revealed after the Click reaction with the commercial EdU Click-It kit (ThermoFisher).

Retrograde axonal tract tracing

NBT electroporation was used for retrograde and anterograde neuronal tracing in gecko embryos (stages E45 to E60). A 5% NBT solution in phosphate buffer was injected into target regions—such as the rotundus, medialis, and dorsal thalamic nuclei or the dorsal ventricular ridge and dorsal cortex—to label sensory circuits. Injection used artificial cerebrospinal fluid (aCSF) with controlled ionic composition, and electroporation (200 unipolar pulses, 50 V) facilitated tracer entry through axonal membranes. After tracing, brains were cultured in oxygenated aCSF for 24 hours, fixed with 4% PFA, and processed for immunohistochemistry using streptavidin Alexa Fluor 488 to visualize NBT distribution.

BirthSeq

Isolation of birthdated cells for scRNA-seq was performed as previously described (*60*). Briefly, chick and mouse embryos were birthdated at early neurogenic timepoints (E4 or E12, respectively) and sacrificed either 2 or 11 days after EdU injection. Birthdated cells were sorted by fluorescence-activated cell sorting from E14 mouse embryos, P3 mouse postnatal pups, and E6 and E15 chick embryos and were prepared for single-cell capture of cells on 10X Genomics platform.

Data integration and clustering

The sequenced FASTQs were aligned and demultiplexed with 10X CellRanger v6.0.2. Afterward, data matrices were imported to R (v4.1.0), where Seurat (v4.1.0) (*66*) was used to further analysis. Cell cycle and mitochondrial percentages were both corrected through the ScaleData() function for cluster identification and SCTransform() for cross-species comparisons. The initial atlases were generated with subtle modifications of Seurat default parameters and functions at several low and high resolutions. To identify cell types, differential gene markers and scientific literature [in situ hybridization databases, our own experiments, and single-cell equivalent experiments from the literature (*58*, *93*–*95*)] were used. This process was followed again after nonneural cells were subset to obtain the final neural atlases. These atlases were used for cross-species comparisons filtered by one-to-one orthologs (based on biomaRt tables, Ensembl) with the four complementary statistical analysis methods: multispecies integration, cluster-specific DE module expression analysis, GSI correlation (*11*), and label transfer (*67*) (see supplementary materials and methods for details).

In situ hybridization

Gecko embryonic brains were fixed in PFA for 10 to 20 hours and subsequently cut in a vibrating microtome in 50-μm-thick sections. M13 forward (5′GCCAGGGTTTTCCCAGTCAC3′) and M13 reverse (5′GGAAACAGCTATGACCATG3′) primers were used to obtain the fragments from our cloned genes that were used to get riboprobes. Sense and antisense digoxygenin-11-UTP-labeled (Roche) riboprobes were synthesized according to the detailed procedures previously described (*96*).

In situ sequencing

Brains were processed according to the direct RNA ISS method published in (*97*). Imaging was performed by a cyclic combinatorial labeling strategy as described in (*98*). After the last round of combinatorial imaging, the probes were stripped and EdU was labeled using a cross-reactive BrdU antibody. The acquired images were processed, denoised, and decoded using the scripts from (*97*) and deposited at https://github.com/Moldia/Lee_2023. The decoded gene expression data were assigned to individual cells based on close proximity to the nearest 4′,6-diamidino-2-phenylindole (DAPI) signal, using StarDist as a segmentation method (*99*). Cell-by-gene expression data were filtered to remove cells with low read counts or suspected doublets and then were integrated with the scRNA-seq datasets using probabilistic cell typing (*100*). The DAPI-based segmentation mask generated by StarDist was applied to the EdU images, and the staining intensity was extracted for each nucleus, as described in (*60*).

Mathematical models

Random continuous Hopfield networks of N = 4000 neurons for mouse and $2N$ neurons for chick were created, representing pallial circuits at birth (end of E18 for mouse, end of E10 for chick). Connections were randomly wired with probability (p = 0.6) and weights distributed by Normal (0, g_r) and Normal (0, g_x) for intra- versus interregion connections, respectively (g_r = 3.0, g_x = 1.5). Neurogenesis was modeled backward in time by random neuron removal based on a Poisson process with region-specific time-dependent rates obtained by spline fitting of experimental data (see data S2 for details). Analysis of the leading eigenvalue followed (*101*).

REFERENCES AND NOTES

1. K. D. Harris, G. M. G. Shepherd, The neocortical circuit: Themes and variations. *Nat. Neurosci.* **18**, 170–181 (2015). doi: 10.1038/nn.3917; pmid: 25622573
2. V. B. Mountcastle, The columnar organization of the neocortex. *Brain* **120**, 701–722 (1997). doi: 10.1093/brain/120.4.701; pmid: 9153131

3. S. Lefort, C. Tomm, J. C. Floyd Sarria, C. C. H. Petersen, The excitatory neuronal network of the C2 barrel column in mouse primary somatosensory cortex. *Neuron* **61**, 301–316 (2009). doi: 10.1016/j.neuron.2008.12.020; pmid: 19186171
4. J. Dugas-Ford, C. W. Ragsdale, Levels of homology and the problem of neocortex. *Annu. Rev. Neurosci.* **38**, 351–368 (2015). doi: 10.1146/annurev-neuro-071714-033911; pmid: 26154980
5. G. F. Striedter, R. G. Northcutt, The independent evolution of dorsal pallia in multiple vertebrate lineages. *Brain Behav. Evol.* **96**, 200–211 (2022). doi: 10.1159/000516563; pmid: 34175847
6. B. M. Colquitt, D. P. Merullo, G. Konopka, T. F. Roberts, M. S. Brainard, Cellular transcriptomics reveals evolutionary identities of songbird vocal circuits. *Science* **371**, eabd9704 (2021). doi: 10.1126/science.abd9704; pmid: 33574185
7. Y. Wang, A. Brzozowska-Prechtl, H. J. Karten, Laminar and columnar auditory cortex in avian brain. *Proc. Natl. Acad. Sci. U.S.A.* **107**, 12676–12681 (2010). doi: 10.1073/pnas.1006645107; pmid: 20616034
8. N. O. E. Krützfeldt, J. M. Wild, Definition and novel connections of the entopallium in the pigeon (*Columba livia*). *J. Comp. Neurol.* **490**, 40–56 (2005). doi: 10.1002/cne.20627; pmid: 16041718
9. S. D. Briscoe, C. B. Albertin, J. J. Rowell, C. W. Ragsdale, Neocortical association cell types in the forebrain of birds and alligators. *Curr. Biol.* **28**, 686–696.e6 (2018). doi: 10.1016/j.cub.2018.01.036; pmid: 29456143
10. C. C. Chen, C. M. Winkler, A. R. Pfenning, E. D. Jarvis, Molecular profiling of the developing avian telencephalon: Regional timing and brain subdivision continuities. *J. Comp. Neurol.* **521**, 3666–3701 (2013). doi: 10.1002/cne.23406; pmid: 23818174
11. M. A. Tosches *et al*., Evolution of pallium, hippocampus, and cortical cell types revealed by single-cell transcriptomics in reptiles. *Science* **360**, 881–888 (2018). doi: 10.1126/science.aar4237; pmid: 29724907
12. T. Nomura, W. Yamashita, H. Gotoh, K. Ono, Species-specific mechanisms of neuron subtype specification reveal evolutionary plasticity of amniote brain development. *Cell Rep.* **22**, 3142–3151 (2018). doi: 10.1016/j.celrep.2018.02.086; pmid: 29562171
13. A. Calabrese, S. M. N. Woolley, Coding principles of the canonical cortical microcircuit in the avian brain. *Proc. Natl. Acad. Sci. U.S.A.* **112**, 3517–3522 (2015). doi: 10.1073/pnas.1408545112; pmid: 25691736
14. M. Stacho *et al*., A cortex-like canonical circuit in the avian forebrain. *Science* **369**, eabc5534 (2020). doi: 10.1126/science.abc5534; pmid: 32973004
15. H. J. Karten, Neocortical evolution: Neuronal circuits arise independently of lamination. *Curr. Biol.* **23**, R12–R15 (2013). doi: 10.1016/j.cub.2012.11.013; pmid: 23305661
16. L. Puelles, Thoughts on the development, structure and evolution of the mammalian and avian telencephalic pallium. *Philos. Trans. R. Soc. London Ser. B* **356**, 1583–1598 (2001). doi: 10.1098/rstb.2001.0973; pmid: 11604125
17. L. Puelles, Comments on the updated tetrapartite pallium model in the mouse and chick, featuring a homologous claustro-insular complex. *Brain Behav. Evol.* **90**, 171–189 (2017). doi: 10.1159/000479782; pmid: 28988246
18. S. J. Gould, Ontogeny and phylogeny—Revisited and reunited. *BioEssays* **14**, 275–279 (1992). doi: 10.1002/bies.950140413; pmid: 1596276
19. F. García-Moreno, Z. Molnár, Variations of telencephalic development that paved the way for neocortical evolution. *Prog. Neurobiol.* **194**, 101865 (2020). doi: 10.1016/j.pneurobio.2020.101865; pmid: 32526253
20. B. Källén, *Embryological Studies on the Nuclei and Their Homologization in the Vertebrate Forebrain* (Gleerup, 1951).
21. R. Nieuwenhuys, L. Puelles, *Towards a New Neuromorphology* (Springer, 2015).
22. P. Gao, K. T. Sultan, X. J. Zhang, S. H. Shi, Lineage-dependent circuit assembly in the neocortex. *Development* **140**, 2645–2655 (2013). doi: 10.1242/dev.087668; pmid: 23757410
23. S. He, Z. Li, S. Ge, Y. C. Yu, S. H. Shi, Inside-out radial migration facilitates lineage-dependent neocortical microcircuit assembly. *Neuron* **86**, 1159–1166 (2015). doi: 10.1016/j.neuron.2015.05.002; pmid: 26050035
24. Y.-C. Yu, R. S. Bultje, X. Wang, S.-H. Shi, Specific synapses develop preferentially among sister excitatory neurons in the neocortex. *Nature* **458**, 501–504 (2009). doi: 10.1038/nature07722; pmid: 19204731
25. E. Rueda-Alaña, F. García-Moreno, Time in neurogenesis: Conservation of the developmental formation of the cerebellar circuitry. *Brain Behav. Evol.* **97**, 33–47 (2022). doi: 10.1159/000519068; pmid: 34592741
26. N. O. E. Krützfeldt, J. M. Wild, Definition and connections of the entopallium in the zebra finch (*Taeniopygia guttata*). *J. Comp. Neurol.* **468**, 452–465 (2004). doi: 10.1002/cne.10972; pmid: 14681937
27. H. Zeier, H. J. Karten, The archistriatum of the pigeon: Organization of afferent and efferent connections. *Brain Res.* **31**, 313–326 (1971). doi: 10.1016/0006-8993(71)90185-5; pmid: 5569153
28. H. M. Tsai, B. B. Garber, L. M. H. Larramendi, 3H-thymidine autoradiographic analysis of telencephalic histogenesis in the chick embryo: II. Dynamics of neuronal migration, displacement, and aggregation. *J. Comp. Neurol.* **198**, 293–306 (1981). doi: 10.1002/cne.901980208; pmid: 7240447
29. I. K. Suzuki, T. Hirata, A common developmental plan for neocortical gene-expressing neurons in the pallium of the domestic chicken *Gallus gallus domesticus* and the Chinese softshell turtle *Pelodiscus sinensis*. *Front. Neuroanat.* **8**, 20 (2014). doi: 10.3389/fnana.2014.00020; pmid: 24778607
30. R. Tremblay, S. Lee, B. Rudy, GABAergic Interneurons in the neocortex: From cellular properties to circuits. *Neuron* **91**, 260–292 (2016). doi: 10.1016/j.neuron.2016.06.033; pmid: 27477017
31. S. J. B. Butt *et al*., The temporal and spatial origins of cortical interneurons predict their physiological subtype. *Neuron* **48**, 591–604 (2005). doi: 10.1016/j.neuron.2005.09.034; pmid: 16301176
32. X. Xu, K. D. Roby, E. M. Callaway, Immunochemical characterization of inhibitory mouse cortical neurons: Three chemically distinct classes of inhibitory cells. *J. Comp. Neurol.* **518**, 389–404 (2010). doi: 10.1002/cne.22229; pmid: 19950390
33. M. X. Moreau, Y. Saillour, A. W. Cwetsch, A. Pierani, F. Causeret, Single-cell transcriptomics of the early developing mouse cerebral cortex disentangle the spatial and temporal components of neuronal fate acquisition. *Development* **148**, dev197962 (2021). doi: 10.1242/dev.197962; pmid: 34170322
34. P. Gao *et al*., Deterministic progenitor behavior and unitary production of neurons in the neocortex. *Cell* **159**, 775–788 (2014). doi: 10.1016/j.cell.2014.10.027; pmid: 25417155
35. F. García-Moreno *et al*., Absence of tangentially migrating glutamatergic neurons in the developing avian brain. *Cell Rep.* **22**, 96–109 (2018). doi: 10.1016/j.celrep.2017.12.032; pmid: 29298437
36. N. Moreno, A. González, S. Rétaux, Development and evolution of the subpallium. *Semin. Cell Dev. Biol.* **20**, 735–743 (2009). doi: 10.1016/j.semcdb.2009.04.008; pmid: 19374952
37. A. L. Garda, L. Puelles, J. L. R. Rubenstein, L. Medina, Expression patterns of Wnt8b and Wnt7b in the chicken embryonic brain suggest a correlation with forebrain patterning centers and morphogenesis. *Neuroscience* **113**, 689–698 (2002). doi: 10.1016/S0306-4522(02)00171-9; pmid: 12150789
38. L. Puelles *et al*., Radial derivatives of the mouse ventral pallium traced with *Dbx1*-LacZ reporters. *J. Chem. Neuroanat.* **75**, 2–19 (2016). doi: 10.1016/j.jchemneu.2015.10.011; pmid: 26748312
39. F. Lamanna *et al*., A lamprey neural cell type atlas illuminates the origins of the vertebrate brain. *Nat. Ecol. Evol.* **7**, 1714–1728 (2023). doi: 10.1038/s41559-023-02170-1; pmid: 37710042
40. J. Woych *et al*., Cell-type profiling in salamanders identifies innovations in vertebrate forebrain evolution. *Science* **377**, eabp9186 (2022). doi: 10.1126/science.abp9186; pmid: 36048957
41. H. Bruguier *et al*., In search of common developmental and evolutionary origin of the claustrum and subplate. *J. Comp. Neurol.* **528**, 2956–2977 (2020). doi: 10.1002/cne.24922; pmid: 32266722
42. L. Puelles *et al*., Selective early expression of the orphan nuclear receptor Nr4a2 identifies the claustrum homolog in the avian mesopallium: Impact on sauropsidian/mammalian pallium comparisons. *J. Comp. Neurol.* **524**, 665–703 (2016). doi: 10.1002/cne.23902; pmid: 26400616
43. G. Kim, A. Doupe, Organized representation of spectrotemporal features in songbird auditory forebrain. *J. Neurosci.* **31**, 16977–16990 (2011). doi: 10.1523/JNEUROSCI.2003-11.2011; pmid: 22114268
44. E. D. Jarvis *et al*., Global view of the functional molecular organization of the avian cerebrum: Mirror images and functional columns. *J. Comp. Neurol.* **521**, 3614–3665 (2013). doi: 10.1002/cne.23404; pmid: 23818122
45. A. Reiner *et al*., Revised nomenclature for avian telencephalon and some related brainstem nuclei. *J. Comp. Neurol.* **473**, 377–414 (2004). doi: 10.1002/cne.20118; pmid: 15116397
46. L. Puelles, M. Martinez-de-la-Torre, S. Martinez, C. Watson, G. Paxinos, *The Chick Brain in Stereotaxic Coordinates and Alternate Stains* (Elsevier, ed. 2, 2018).
47. J. Dugas-Ford, J. J. Rowell, C. W. Ragsdale, Cell-type homologies and the origins of the neocortex. *Proc. Natl. Acad. Sci. U.S.A.* **109**, 16974–16979 (2012). doi: 10.1073/pnas.1204773109; pmid: 23027930
48. A. Reiner, H. J. Karten, The laminar source of efferent projections from the avian Wulst. *Brain Res.* **275**, 349–354 (1983). doi: 10.1016/0006-8993(83)90996-4; pmid: 6194858
49. T. Shimizu, K. Cox, H. J. Karten, Intratelencephalic projections of the visual wulst in pigeons (*Columba livia*). *J. Comp. Neurol.* **359**, 551–572 (1995). doi: 10.1002/cne.903590404; pmid: 7499547
50. R. Nieuwenhuys, H. J. Donkelar, C. Nicholson, *The Central Nervous System of Vertebrates* (Springer, 1998). doi: 10.1007/978-3-642-18262-4
51. T. Nomura, M. Kawaguchi, K. Ono, Y. Murakami, Reptiles: A new model for brain evo-devo research. *J. Exp. Zool. B Mol. Dev. Evol.* **320**, 57–73 (2013). doi: 10.1002/jez.b.22484; pmid: 23319423
52. L. L. Bruce, A. B. Butler, Telencephalic connections in lizards. II. Projections to anterior dorsal ventricular ridge. *J. Comp. Neurol.* **229**, 602–615 (1984). doi: 10.1002/cne.902290412; pmid: 6209314
53. C. D. Balaban, P. S. Ulinski, Organization of thalamic afferents to anterior dorsal ventricular ridge in turtles. I. Projections of thalamic nuclei. *J. Comp. Neurol.* **200**, 95–129 (1981). doi: 10.1002/cne.902000108; pmid: 7251947
54. F. Martínez-Garcíaa, M. Amiguet, W. K. Schwerdtfeger, F. E. Olucha, M. J. Lorente, Interhemispheric connections through the pallial commissures in the brain of *Podarcis hispanica* and *Gallotia stehlinii* (Reptilia, Lacertidae). *J. Morphol.* **205**, 17–31 (1990). doi: 10.1002/jmor.1052050104; pmid: 29865699
55. P. V. Hoogland, E. Vermeulen-Vanderzee, Efferent connections of the dorsal cortex of the lizard *Gekko gecko* studied with *Phaseolus vulgaris*-leucoagglutinin. *J. Comp. Neurol.* **285**, 289–303 (1989). doi: 10.1002/cne.902850302; pmid: 2760266
56. L. L. Bruce, A. B. Butler, Telencephalic connections in lizards. I. Projections to cortex. *J. Comp. Neurol.* **229**, 585–601 (1984). doi: 10.1002/cne.902290411; pmid: 6209313
57. L. Telley *et al*., Sequential transcriptional waves direct the differentiation of newborn neurons in the mouse neocortex. *Science* **351**, 1443–1446 (2016). doi: 10.1126/science.aad8361; pmid: 26940868
58. D. J. Di Bella *et al*., Molecular logic of cellular diversification in the mouse cerebral cortex. *Nature* **595**, 554–559 (2021). doi: 10.1038/s41586-021-03670-5; pmid: 34163074
59. D. Hain *et al*., Molecular diversity and evolution of neuron types in the amniote brain. *Science* **377**, eabp8202 (2022). doi: 10.1126/science.abp8202; pmid: 36048944
60. E. Rueda-Alaña *et al*., BirthSeq, a new method to isolate and analyze dated cells in different vertebrates. *Development* **151**, dev202429 (2024). doi: 10.1242/dev.202429; pmid: 38856078
61. J. A. de Carlos, L. López-Mascaraque, F. Valverde, Dynamics of cell migration from the lateral ganglionic eminence in the rat. *J. Neurosci.* **16**, 6146–6156 (1996). doi: 10.1523/JNEUROSCI.16-19-06146.1996; pmid: 8815897
62. I. Cobos, L. Puelles, S. Martínez, The avian telencephalic subpallium originates inhibitory neurons that invade tangentially the pallium (dorsal ventricular ridge and cortical areas). *Dev. Biol.* **239**, 30–45 (2001). doi: 10.1006/dbio.2001.0422; pmid: 11784017
63. Z. Yao *et al*., A taxonomy of transcriptomic cell types across the isocortex and hippocampal formation. *Cell* **184**, 3222–3241.e26 (2021). doi: 10.1016/j.cell.2021.04.021; pmid: 34004146
64. F. García-Moreno, L. López-Mascaraque, J. A. De Carlos, Origins and migratory routes of murine Cajal-Retzius cells. *J. Comp. Neurol.* **500**, 419–432 (2007). doi: 10.1002/cne.21128; pmid: 17120279
65. F. Bielle *et al*., Multiple origins of Cajal-Retzius cells at the borders of the developing pallium. *Nat. Neurosci.* **8**, 1002–1012 (2005). doi: 10.1038/nn1511; pmid: 16041369

66. Y. Hao *et al*., Integrated analysis of multimodal single-cell data. *Cell* **184**, 3573–3587.e29 (2021). doi: 10.1016/j.cell.2021.04.048; pmid: 34062119
67. T. Stuart *et al*., Comprehensive integration of single-cell data. *Cell* **177**, 1888–1902.e21 (2019). doi: 10.1016/j.cell.2019.05.031; pmid: 31178118
68. B. Van de Sande *et al*., A scalable SCENIC workflow for single-cell gene regulatory network analysis. *Nat. Protoc.* **15**, 2247–2276 (2020). doi: 10.1038/s41596-020-0336-2; pmid: 32561888
69. S. D. Briscoe, C. W. Ragsdale, Homology, neocortex, and the evolution of developmental mechanisms. *Science* **362**, 190–193 (2018). doi: 10.1126/science.aau3711; pmid: 30309947
70. B. Zaremba *et al*., Developmental origins and evolution of pallial cell types and structures in birds. *Science* **387**, eadp5182 (2025). doi: 10.1126/science.aau3711; pmid: 30309947
71. O. Güntürkün, K. von Eugen, J. Packheiser, R. Pusch, Avian pallial circuits and cognition: A comparison to mammals. *Curr. Opin. Neurobiol.* **71**, 29–36 (2021). doi: 10.1016/j.conb.2021.08.007; pmid: 34562800
72. A. G. Blankenship, M. B. Feller, Mechanisms underlying spontaneous patterned activity in developing neural circuits. *Nat. Rev. Neurosci.* **11**, 18–29 (2010). doi: 10.1038/nrn2759; pmid: 19953103
73. M. Li *et al*., Synaptogenesis in the developing mouse visual cortex. *Brain Res. Bull.* **81**, 107–113 (2010). doi: 10.1016/j.brainresbull.2009.08.028; pmid: 19751806
74. M. Bergmann, D. Grabs, G. Rager, Expression of presynaptic proteins is closely correlated with the chronotopic pattern of axons in the retinotectal system of the chick. *J. Comp. Neurol.* **418**, 361–372 (2000). doi: 10.1002/(SICI)1096-9861(20000313)418:3<361::AID-CNE9>3.0.CO;2-U; pmid: 10701832
75. L. George, J. Kasemeier-Kulesa, B. R. Nelson, N. Koyano-Nakagawa, F. Lefcort, Patterned assembly and neurogenesis in the chick dorsal root ganglion. *J. Comp. Neurol.* **518**, 405–422 (2010). doi: 10.1002/cne.22248; pmid: 20017208
76. F. J. Martini, T. Guillamón-Vivancos, V. Moreno-Juan, M. Valdeolmillos, G. López-Bendito, Spontaneous activity in developing thalamic and cortical sensory networks. *Neuron* **109**, 2519–2534 (2021). doi: 10.1016/j.neuron.2021.06.026; pmid: 34293296
77. I. Gutman, *Algebraic Combinatorics and Applications*, A. Betten, A. Kohnert, R. Laue, A. Wassermann, Eds. (Springer, 2001), pp. 196–211.doi: 10.1007/978-3-642-59448-9_13
78. Y. Murakami, K. Uchida, F. M. Rijli, S. Kuratani, Evolution of the brain developmental plan: Insights from agnathans. *Dev. Biol.* **280**, 249–259 (2005). doi: 10.1016/j.ydbio.2005.02.008; pmid: 15882571
79. G. Gedman *et al*., As above, so below: Whole transcriptome profiling demonstrates strong molecular similarities between avian dorsal and ventral pallial subdivisions. *J. Comp. Neurol.* **529**, 3222–3246 (2021). doi: 10.1002/cne.25159; pmid: 33871048
80. P. Rakic, Guidance of neurons migrating to the fetal monkey neocortex. *Brain Res.* **33**, 471–476 (1971). doi: 10.1016/0006-8993(71)90119-3; pmid: 5002632
81. F. García-Moreno, Z. Molnár, Subset of early radial glial progenitors that contribute to the development of callosal neurons is absent from avian brain. *Proc. Natl. Acad. Sci. U.S.A.* **112**, E5058–E5067 (2015). doi: 10.1073/pnas.1506377112; pmid: 26305942
82. F. García-Moreno, N. A. Vasistha, J. Begbie, Z. Molnár, CLoNe is a new method to target single progenitors and study their progeny in mouse and chick. *Development* **141**, 1589–1598 (2014). doi: 10.1242/dev.105254; pmid: 24644261
83. S. C. Noctor, V. Martínez-Cerdeño, L. Ivic, A. R. Kriegstein, Cortical neurons arise in symmetric and asymmetric division zones and migrate through specific phases. *Nat. Neurosci.* **7**, 136–144 (2004). doi: 10.1038/nn1172; pmid: 14703572
84. N. A. Vasistha *et al*., Cortical and clonal contribution of Tbr2 expressing progenitors in the developing mouse brain. *Cereb. Cortex* **25**, 3290–3302 (2015). doi: 10.1093/cercor/bhu125; pmid: 24927931
85. A. Cárdenas *et al*., Evolution of cortical neurogenesis in amniotes controlled by Robo signaling levels. *Cell* **174**, 590–606.e21 (2018). doi: 10.1016/j.cell.2018.06.007; pmid: 29961574
86. N. Hecker *et al*., Enhancer-driven cell type comparison reveals similarities between the mammalian and bird pallium. *Science* **387**, eadp3957 (2025). doi: 10.1126/science.aau3711; pmid: 30309947
87. K. Lust *et al*., Single-cell analyses of axolotl telencephalon organization, neurogenesis, and regeneration. *Science* **377**, eabp9262 (2022). doi: 10.1126/science.abp9262; pmid: 36048956
88. C. H. Waddington, Canalization of development and the inheritance of acquired characters. *Nature* **150**, 563–565 (1942). doi: 10.1038/150563a0
89. M. L. Siegal, A. Bergman, Waddington's canalization revisited: Developmental stability and evolution. *Proc. Natl. Acad. Sci. U.S.A.* **99**, 10528–10532 (2002). doi: 10.1073/pnas.102303999; pmid: 12082173
90. N. Yamamoto *et al*., A new interpretation on the homology of the teleostean telencephalon based on hodology and a new eversion model. *Brain Behav. Evol.* **69**, 96–104 (2007). doi: 10.1159/000095198; pmid: 17230017
91. H. Ito, N. Yamamoto, Non-laminar cerebral cortex in teleost fishes? *Biol. Lett.* **5**, 117–121 (2009). doi: 10.1098/rsbl.2008.0397; pmid: 18832057
92. E. Rueda-Alaña, I. Martínez-Garay, J. M. Encinas, Z. Molnár, F. García-Moreno, Dbx1-derived pyramidal neurons are generated locally in the developing murine neocortex. *Front. Neurosci.* **12**, 792 (2018). doi: 10.3389/fnins.2018.00792; pmid: 30429769
93. L. Telley *et al*., Temporal patterning of apical progenitors and their daughter neurons in the developing neocortex. *Science* **364**, eaav2522 (2019). doi: 10.1126/science.aav2522; pmid: 31073041
94. R. C. Bandler *et al*., Single-cell delineation of lineage and genetic identity in the mouse brain. *Nature* **601**, 404–409 (2022). doi: 10.1038/s41586-021-04237-0; pmid: 34912118
95. Z. Li *et al*., Transcriptional priming as a conserved mechanism of lineage diversification in the developing mouse and human neocortex. *Sci. Adv.* **6**, eabd2068–15 (2020). doi: 10.1126/sciadv.abd2068; pmid: 33158872
96. J. Ferran *et al*., in *In Situ Hybridization Methods*, vol. 99, G. Hauptmann, Ed. (Humana Press, 2015), pp. 61–82. doi: 10.1007/978-1-4939-2303-8_4
97. H. Lee *et al*., Open-source, high-throughput targeted in situ transcriptomics for developmental and tissue biology. *Development* **151**, dev202448 (2024). doi: 10.1242/dev.202448; pmid: 39099456
98. D. Gyllborg *et al*., Hybridization-based in situ sequencing (HybISS) for spatially resolved transcriptomics in human and mouse brain tissue. *Nucleic Acids Res.* **48**, e112 (2020). doi: 10.1093/nar/gkaa792; pmid: 32990747
99. U. Schmidt, M. Weigert, C. Broaddus, G. Myers, "Cell detection with star-convex polygons" in *Medical Image Computing and Computer Assisted Intervention – MICCAI 2018*, Lecture Notes in Computer Science, vol. 11071, A. Frangi, J. Schnabel, C. Davatzikos, C. Alberola-López, G. Fichtinger, Eds. (Springer, 2018). doi: 10.1007/978-3-030-00934-2_30
100. X. Qian *et al*., Probabilistic cell typing enables fine mapping of closely related cell types in situ. *Nat. Methods* **17**, 101–106 (2020). doi: 10.1038/s41592-019-0631-4; pmid: 31740815
101. J. Aljadeff, M. Stern, T. Sharpee, Transition to chaos in random networks with cell-type-specific connectivity. *Phys. Rev. Lett.* **114**, 088101 (2015). doi: 10.1103/PhysRevLett.114.088101; pmid: 25768781

ACKNOWLEDGMENTS

We thank L. Kratochvil for their contribution, which allowed for the establishment of our gecko colony; Z. Molnár and S. Butt (University of Oxford, UK) and J. R. Pineda (Achucarro, Spain) for productive initial comments that led to the current project; H. Kaessmann and B. Zaremba (Heidelberg University, Germany) for creative and helpful comments on the manuscript; M. Aguilera (Basque Center for Applied Mathematics, Spain) for insightful conversations on the Hopfield networks; the Servicio General de Microscopía Analítica y de Alta Resolución en Biomedicina, SGIker at the UPV/EHU; and the ISS unit at SciLifeLab, who provided some ISS imaging data. We also thank those many researchers who have discussed the data with our team over all these years. **Funding:** This work was funded by a Ikerbasque Research Fellowship to F.G.-M.; Spanish Ministry grants MICINN PGC2018-096173-A-I00 and MICINN PID2021-125156NB-I00 F.G.-M; Basque Government grants PIBA 2020_1_0057 and PIBA_2022_1_0027 to F.G.-M.; EASI-GENOMICS 3rd TNA call PID14596 grant to F.G.-M.; Krembil Foundation Seed Fund FCC410015233 to M.D.P.; Spanish Ministry of Science, Innovation, and Universities (MCIU), State Research Agency (AEI), and European Regional Development Fund (FEDER), PGC2018-098229-B-100 to J.L.F.; Séneca Foundation 21903/PI/22 to J.L.F.; Chan Zuckerberg Initiative – Advised fund of Silicon Valley Community Foundation grant DAF2018-191929 to M.N.; Erling-Persson Family Foundation – A human developmental cell atlas grant to M.N.; Knut and Alice Wallenberg Foundation grant KAW 2018.0172 to M.N.; Swedish Research Council grant 2019-01238 to M.N.; Swedish Cancer Society – Cancerfonden grant CAN 2021/1726 to M.N.; Spanish Ministry grants MINECO/MICINN SAF-2015-70866-R and MICINN PID2019-104766RB to J.M.E.-P. Basque Government grant PIBA_2021_1_0018 to J.M.E.-P.; and a Fundacion Tatiana predoctoral fellowship to R. S.-G. CIC bioGUNE support was provided by the Department of Industry, Tourism and Trade of the Government of the Autonomous Community of the Basque Country (Emaitek and Elkartek Research Programs 2015-2023, KK-2020/00008), the Innovation Technology Department of the Bizkaia County, and by the Spanish Ministry of Science and Innovation grant MCIN/AEI/10.13039/501100011033 (PID2020-118464RB I00 and Severo Ochoa Excellence Accreditation CEX2021-001136-S) to A.M.A. and M.d.V. **Author contributions:** E.R.-A. and F.G.-M. conceived the project, interpreted the data, designed and performed experiments and data analysis, and wrote the manuscript with input from all authors. T.G.-F., A.O.-M., and A.F. performed embryo work and experiments. A.M.A., A.B., and A.Q. performed scRNA-seq. E.V. and R.S.-G. performed bioinformatic analysis. L.E., M.R., and M.d.V. performed FACS sorting analysis. M.G., S.M.-S., and E.R.-A. performed and analyzed the in situ sequencing experiments. J.L.F., D.G., and Á.T. performed and analyzed in situ hybridization. M.D.P. and F.G.-M. performed theoretical modeling and curated the supplementary modeling notes. M.N., A.D., J.M.E.-P., and F.G.-M. provided reagents. **Competing interests:** M.G. and S.M.-S. are co-founders of Spatialist, a company focused on data analysis for spatial-omics. All other authors declare no competing interests. **Data and materials availability:** Data generated for this study have been submitted to the National Center for Biotechnology Information (NCBI) Gene Expression Omnibus (GEO; https://www.ncbi.nlm.nih.gov/geo/) under accession number GSE271958. The code used for analysis (scRNA-seq processing, interspecies comparisons, and spatial transcriptomics) can be found at https://github.com/phylobrain/Rueda-Alana2024.

SUPPLEMENTARY MATERIALS

Submitted 9 April 2024; accepted 20 November 2024
10.1126/science.adp3411